An Adaptable Passive Lower-Limb Prosthesis

Citation

Permanent link

Terms of Use

Share Your Story

An Adaptable Passive Lower-Limb Prosthesis for Pediatric Amputees

by

Alexander Yang

Submitted to the Harvard John A. Paulson School of Engineering and
Applied Sciences
in partial fulfillment of the requirements for the degree of

Bachelor of Science in Engineering Sciences

at

HARVARD UNIVERSITY

March 2017

Certified by...

Tyler Clites

PhD Student, Harvard-MIT HST

Thesis Supervisor

Certified by...

Hugh Herr

Associate Professor, MIT Media Arts and Sciences

Thesis Supervisor

Certified by...

Christopher Lombardo

Lecturer, Harvard School of Engineering and Applied Sciences

Thesis Supervisor

Certified by...

Maurice Smith

Professor, Harvard School of Engineering and Applied Sciences

Thesis Supervisor

An Adaptable Passive Lower-Limb Prosthesis for Pediatric Amputees

by

Alexander Yang

Abstract

While the need for rigorous and affordable prostheses in developing countries is serious, little to none of these devices exist and are available to lower-limb amputees. In addition, pediatric amputees in low-income areas are further prohibited from accessing these technologies; the rapid growth rate of their limbs calls for frequent replacements of prostheses, making existing solutions economically unfeasible.

In this thesis, a model was generated to depict how the kinematic and kinetics of healthy pediatric gait vary with age. This model was then used to optimize the design of a passive ankle prosthesis, which uses a spring and damper system to store and release energy to the ankle joint. Most importantly, this system was designed to adapt to the changing gait pattern and dynamics of a pediatric amputee.

The presented paradigm—using a computer model to efficiently predict the gait produced by various prosthesis design—allows for the creation of affordable, accurate, and tailored devices for individuals who currently are forced to settle for one-size-fits-all passive solutions. This approach promises to substantially increase the access to prostheses for children around the world.

Thesis Supervisor: Tyler Clites
Title: PhD Student, Harvard-MIT HST

Thesis Supervisor: Hugh Herr
Title: Associate Professor, MIT Media Arts and Sciences

Thesis Supervisor: Christopher Lombardo
Title: Lecturer, Harvard School of Engineering and Applied Sciences

Thesis Supervisor: Maurice Smith
Title: Professor, Harvard School of Engineering and Applied Sciences

Contents

List of Figures

List of Tables

Chapter 1

Introduction

While global health has largely focused on addressing communicable disease challenges, little has been done in the area of disability. Understandably, relieving the global disability burden requires solutions more tailored to the specific needs of an individual patient, making the field less attractive than HIV or malaria prevention, for example. As a result, the amputee burden still remains. The specific number of patients in need of a limb is unclear, as little disability data exists pertaining to developing countries. The WHO estimates that 0.5% of a given population is in need of a prosthesis [1]. Using this figure, about 25.5 million people in Africa, Asia, and Latin America would benefit from access to an artificial limb.

While many are working on ways to deliver affordable lower limb prostheses to adults around the world, few have addressed the pediatric space. The primary reason is the fact that children are still growing, and thus a prosthesis optimally fitted for a child may not perform as well with time. Obtaining a new prosthesis as soon as the child has outgrown the old one is not economically viable for families in low-resource settings. With around 1 million children (under the age of 18) globally who are in need of a prosthesis, new devices that are built around novel design, delivery and use models are increasingly necessary [1].

The objective for this thesis was to build an affordable pediatric passive ankle prosthesis that can be easily adjusted mechanically in order to continually perform optimally, eliminating the need to replace the prosthesis with time. This project will

incorporate a modeling, a prototype construction, and a testing component.

The target user for this project will be prosthetic clinics/global health organizations based in developing countries looking to purchase affordable prostheses to distribute or sell to pediatric amputees. Patients in developing countries often choose to forgo treatment because prostheses are too costly and clinics that have begun distributing devices for free are underfunded and backlogged [2]. Pediatric patients are even more forgotten because providing them with prostheses over adult patients is not economically favorable [2].

A specific example of these organizations is Exceed, a non-profit operating in Southeast Asia that both trains prosthetists and funds clinics providing free prostheses to amputees [3]. Having worked with one of these clinics in Cambodia, both their burden of pediatric patients as well as their willingness to test new approaches and devices makes Exceed a strong champion of this project.

Chapter 2

Background Research

2.1 Existing Prostheses

2.1.1 Active Devices

The leading ankle prosthesis today was designed by Prof. Hugh Herr from the MIT Media Lab. The BiOM (Figure 2-1) has been made to address the most pressing disadvantage of standard carbon ankle prostheses: they are not able to perform net-positive work that a biological Achilles tendon would do for biological ankles [4]. The BiOM, categorized as an active device, makes up for this loss by utilizing a motor, which actively delivers the necessary power to the prosthesis when a biological tendon and muscle normally would. While the device was shown to produce similar joint dynamics compared to biological behavior, at $50,000 a limb, the solution is still prohibitively expensive [5].

2.1.2 Passive Devices

A number of research groups and companies have found ways to developed passive lower-limb prostheses that deliver power to a joint without the use of a motor. Rice, Schimmels, and Huang from Marquette University incorporated a spring and damper system into an assistive device, resulting in a prosthetic that generated 44.5% of the net rotational work performed by a healthy ankle [6]. The group has also filed a

Figure 2-1: Biom ankle prosthesis [4].

patent for the design [7].

In the affordable space, the Stanford-Jaipur Knee (Figure 2-2) has been a pioneer. Based on a simple four-bar linkage geometry, the artificial knee added additional planes of rotation to traditional knee prosthetics, which previously rotated on a single axis [8]. This geometry allowed a more accurate matching of normal human gait. At $20 a device, over 9,250 patients have been fitted since inception in 2009 [9]. The team recently developed a new ankle prosthesis—the Jaipur Foot—that costs $50 [10]. These devices, however, are not designed to provide any power to the knee joint.

Limbs International is a non-profit organization focused on delivering affordable ankle and knee prostheses to low-resource countries. Unlike the Stanford-Jaipur Knee, Limbs International has designed their prosthetic joints to utilize an energy storage and release spring-like mechanism [11].

2.2 Concerns

Although passive devices, due to their affordability, are much more accessible solutions, their primary shortcoming is inaccuracy. Since these devices are unable to deliver sufficient torque to the ankle joint, users of passive devices exhibit gait patterns that differ from those of healthy individuals. These patients have shorter strides and often utilize their sound joints (hip) to compensate for power, resulting in many associated comorbidities [12].

Figure 2-2: Jaipur knee prosthesis [8].

In addition to this concern, none of the existing technologies specifically address pediatric prostheses. Some, like the Stanford-Jaipur Knee and Limbs International device, have produced low-cost devices, but their solutions are designed for a specific limb size and gait pattern. In particular, these devices do not allow for their joint mechanics to be manually adjusted in order to adapt the prosthesis's dynamics as the child grows or gains weight.

Chapter 3

Design Aim

Given the limitations of existing passive prosthetic technologies, there exists an urgent need for a lower-limb device that is capable of human-like dynamics but also adaptable in order to faithfully capture the changing gait pattern of a pediatric amputee as he ages.

Equally important is the affordability of such a device, as the greatest need lies in communities that have the least access to prosthetic technologies. With existing technologies, however, too often do cost and human-like dynamics come hand in hand. The best prostheses are able to deliver sufficient power to the ankle joint at the necessary time during gait, but these devices are often cost-prohibitive.

As discussed in Section 2.1.2, however, spring/damper systems have proven effective in the prosthetic space. Able to store and release energy at controlled moments during gait, spring-loaded devices provide an efficient and affordable way of replacing human joints. Still lacking, however, is the ability of these devices to adapt to growing patients.

Based on these considerations and requirements, device specifications pertaining to four categories—General Requirements, Accuracy, Adaptability and Affordability—were formulated.

3.1 General Requirements

The following requirements refer to the overall construction, strength, dimensions, and weight of the ankle prosthesis.

- Lower limb prosthesis with single DOF (ankle) for trans-tibial pediatric amputees

  - Ankle prosthesis is the simplest lower-limb device to design because only one joint needs to be replaced

- Passive device (no actuators or electronic components) consisting of springs and dampers as core components

- Device should be designed to integrate with standard pyramidal prosthesis adapter [13]

- Prosthesis height should be no greater than 18 cm, measured from the ground to the proximal prosthesis adapter

  - Based on size of conventional Ossur ankle-foot prosthesis [13]

- Device no more than 5% body mass

  - 5% is the average combined body mass fraction of the foot and shank in children [14]

- Able to withstand 7000 N vertical force

  - Average ground reaction force experience by children jumping from 0.3 meters is 4.5 times body weight (SD 1.7) [15]. Given average body weight of sample subjects (40 kg) and safety factor of 4, maximum force permissible is 7000 N

- Device performance requirements limited to walking speed

  - Up to 1.5 m/s (average walking speed in 12 year old children) [16]

3.2 Accuracy

The following requirements use normal pediatric gait as a standard for the device's accuracy.

- Forces and torques at hip and knee in control case are faithfully mimicked in patient

    - Values of forces and torques do not deviate more than 5% from expected

- Resultant joint angles in amputee with prosthesis are within range of motion of joint

- Ankle joint (foot) should be stiff in swing phase of gait

3.3 Adaptability

The following requirements ensure the device achieves its goal of accommodating a range of patient ages.

- Designed to adapt to three age ranges (ranges constrained by available child anthropometric data from literature) [14]

    - 7-8, 9-10, and 11-13

- Mechanical mechanism allowing adaptation to the three age ranges

- Adjustable segment lengths (foot and shank) as well as joint spring/damper parameters

- No tools required to adjust device

- Adjustable by a parent with no medical/prosthetic experience

3.4 Affordability

The following requirements use existing state-of-the-art technologies as a standard for the device's affordability.

- Cost of raw materials less than $50 (based on the cost of a Jaipur Foot)

- Lifespan of device at least 4 years (lifetime of Jaipur Foot) [17]

3.5 Summary

The above design specifications are summarized in Table 3.1.

Functional Requirement	Design Specification	Rationale
Profile	< 18 cm high	Compatible with existing adapters
Weight	< 5% of body mass	Body mass of shank and foot in children
Walking Speed	up to 1.5 m/s	Average walking speed of children
Load	Up to 7000 N vertical force	Average ground reaction force of children jumping from 0.3 m
Accuracy	< 5% deviation of forces and torques from healthy child	Comparable gait pattern to healthy gait
Adaptable	Ages 7-11	Wide range of children
Cost	< $50	Affordable compared to similar products
Lifespan	> 4 years	Durable compared to similar products

Table 3.1: Design Specifications

Chapter 4

Design Approach

In order to design a functional prosthesis, a mathematical model was first built to understand the kinematics and kinetics of healthy pediatric gait at various ages of development. This model was subsequently used to evaluate multiple ankle prosthetic designs as well as determine a set of optimal parameters for the device.

Based on these parameters, an ankle prosthesis was designed in CAD and a prototype was subsequently manufactured.

Finally, testing was performed on the prototype to quantify the performance of the device as well as to evaluate the accuracy of the model and the manufacturing process.

The subsequent chapters outline in detail the modeling, prototyping, and testing processes.

Chapter 5

Gait Model

5.1 Overview

To best characterize healthy pediatric gait, a mathematical model was built to understand variations in joint positions, forces and torques throughout the gait cycle of a child at a particular age. Once this was achieved, the model could be used to explore the effects on gait of introducing an ankle prosthesis.

The human gait is comprised of two distinct phases: stance, during which the foot remains in contact with the ground, and swing, during which it is not. Prior to developing a human gait model, a decision was made to ignore the swing phase, since the foot (and, likewise, an ankle prosthesis) does not apply forces or torques on the ground.

Within the stance phase of the gait cycle, there are additionally two distinct phases, as shown in Figure 5-1: one during which the heel is in contact with the ground and another during which the toe is in contact. These two phases were modeled separately, since a different joint is in contact with the ground in each case.

A mathematical model, using the generalized equations of motion approach, was constructed based on previous unpublished work from Prof. Hugh Herr's Group. Tyler Clites developed a gait model for goats, whose joint positioning differ slightly from that of humans. In addition, the stance phase of a goat's gait cycle only consists of the toe contact phase—a goat's heel is never in contact with the ground.
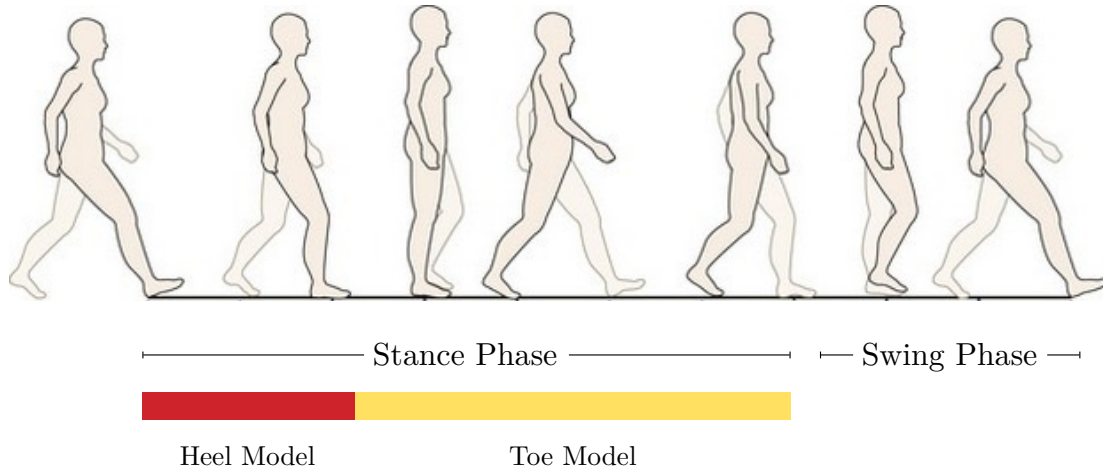
Figure 5-1: Full gait cycle, highlighting phases that were modeled [18].

5.2 Formulation

5.2.1 Toe Model

The toe model was based on a triple-inverted pendulum anchored at the toe. Figure 5-2 shows a schematic of segments involved (thigh, shank, and foot) as well as notation used for the torques and angles at each joint. The angles are defined as absolute, relative to the ground. The torques are defined such that positive values result in limb extension. All measurements are taken in the sagittal plane during normal gait.

Based on Figure 5-2, Equations 5.1-5.3 were written to describe the position and velocity of each limb segment's center of mass, in terms of the lengths of each segment n (l_n), the location of each segment's center of mass as measured from the segment's distal end (r_n), and $\theta_n, \dot{\theta}_n$.

$$x_1 = -r_1 \cos \theta_1$$
$$y_1 = r_1 \sin \theta_1$$
$$\dot{x}_1 = r_1 \sin \theta_1 \dot{\theta}_1 \quad (5.1)$$
$$\dot{y}_1 = r_1 \cos \theta_1 \dot{\theta}_1$$

13
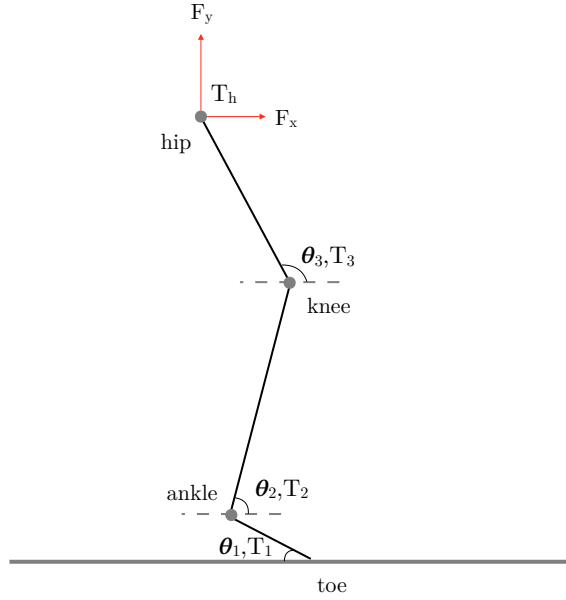
Figure 5-2: Schematic of the Toe Model, showing torque and angle notation for each joint.

$$x_2 = -l_1 \cos\theta_1 + r_2 \cos\theta_2$$

$$y_2 = l_1 \sin\theta_1 + r_2 \sin\theta_2$$

$$\dot{x}_2 = l_1 \sin\theta_1\dot{\theta}_1 - r_2 \sin\theta_2\dot{\theta}_2$$

$$\dot{y}_2 = l_1 \cos\theta_1\dot{\theta}_1 + r_2 \cos\theta_2\dot{\theta}_2$$

(5.2)

$$x_3 = -l_1 \cos\theta_1 + l_2 \cos\theta_2 + r_3 \cos\theta_3$$

$$y_3 = l_1 \sin\theta_1 + l_2 \sin\theta_2 + r_3 \sin\theta_3$$

$$\dot{x}_3 = l_1 \sin\theta_1\dot{\theta}_1 - l_2 \sin\theta_2\dot{\theta}_2 - r_3 \sin\theta_3\dot{\theta}_3$$

$$\dot{y}_3 = l_1 \cos\theta_1\dot{\theta}_1 + l_2 \cos\theta_2\dot{\theta}_2 + r_3 \cos\theta_3\dot{\theta}_3$$

(5.3)

The potential energy of the total leg system is equivalent to the sum of the potential energies of each leg segment, as expressed in Equation 5.4.

$$P = \sum_{i=1}^{3} m_i g y_i$$

(5.4)

Similarly, the total kinetic energy is equal to the sum of the combined inertial

14

energies and rotational energies of each segment, as expressed in Equation 5.5

$$K = \sum_{i=1}^{3} \frac{1}{2} m_i (\dot{x}_i^2 + \dot{y}_i^2) + \frac{1}{2} I_i \dot{\theta}_i^2 \tag{5.5}$$

Using equations 5.4 and 5.5, the Lagrangian can be expressed as follows:

$$\mathcal{L} = K - P$$

Using the Lagrangian, we can write the Lagrangian equations of motion in polar coordinates for each limb segment subject to conservative forces:

$$\bar{Q} = \begin{bmatrix} Q_1 \\ Q_2 \\ Q_3 \end{bmatrix} = \begin{bmatrix} \frac{d}{dt}\left(\frac{\partial \mathcal{L}}{\partial \dot{\theta}_1}\right) - \frac{\partial \mathcal{L}}{\partial \theta_1} \\ \frac{d}{dt}\left(\frac{\partial \mathcal{L}}{\partial \dot{\theta}_2}\right) - \frac{\partial \mathcal{L}}{\partial \theta_2} \\ \frac{d}{dt}\left(\frac{\partial \mathcal{L}}{\partial \dot{\theta}_3}\right) - \frac{\partial \mathcal{L}}{\partial \theta_3} \end{bmatrix} \tag{5.6}$$

The left hand side of Equation 5.6 is equivalent to the non-conservative forces acting on each limb segment, which can be written as:

$$\bar{Q} = \begin{bmatrix} Q_1 \\ Q_2 \\ Q_3 \end{bmatrix} = \begin{bmatrix} T_2 + F_x l_1 \sin\theta_1 + F_y l_1 \cos\theta_1 \\ T_2 - T_3 - F_x l_2 \sin\theta_2 + F_y l_2 \cos\theta_2 \\ T_3 - T_h - F_x l_3 \sin\theta_3 + F_y l_3 \cos\theta_3 \end{bmatrix} \tag{5.7}$$

Combining Equations 5.6 and 5.7 gives us a system of three equations, in terms of $\theta_1, \theta_2, \theta_3, T_1, T_2, T_3, T_h, F_x$, and F_y:

$$
\begin{bmatrix}
\dfrac{d}{dt}\left(\dfrac{\partial \mathcal{L}}{\partial \dot{\theta}_1}\right) - \dfrac{\partial \mathcal{L}}{\partial \theta_1} \\[2ex]
\dfrac{d}{dt}\left(\dfrac{\partial \mathcal{L}}{\partial \dot{\theta}_2}\right) - \dfrac{\partial \mathcal{L}}{\partial \theta_2} \\[2ex]
\dfrac{d}{dt}\left(\dfrac{\partial \mathcal{L}}{\partial \dot{\theta}_3}\right) - \dfrac{\partial \mathcal{L}}{\partial \theta_3}
\end{bmatrix}
=
\begin{bmatrix}
T_2 + F_x l_1 \sin\theta_1 + F_y l_1 \cos\theta_1 \\[1ex]
T_2 - T_3 - F_x l_2 \sin\theta_2 + F_y l_2 \cos\theta_2 \\[1ex]
T_3 - T_h - F_x l_3 \sin\theta_3 + F_y l_3 \cos\theta_3
\end{bmatrix}
\tag{5.8}
$$

$$
\text{where } \mathcal{L} = \sum_{i=1}^{3} \frac{1}{2} m_i(\dot{x}_i^2 + \dot{y}_i^2) + \frac{1}{2} I_i \dot{\theta}_i^2 - \sum_{i=1}^{3} m_i g y_i
$$

Since we have three equations, knowing six of the nine variables would allow us to determine the remaining three at any point in the stance phase during which the toe is in contact with the ground. System of equations 5.8, which forms the structure behind the Toe Model, was implemented in MATLAB.

5.2.2 Heel Model

A model for the heel contact portion of the stance phase was similarly constructed, based on an inverted double pendulum. Figure 5-3 shows a schematic of segments involved (thigh and shank) as well as notation used for the torques and angles at each joint—the naming conventions were similar to those used in Figure 5-2.

Similarly, a system of equations was written. However, only two limb segments were considered, thus resulting in two equations expressed in terms of θ_2, θ_3, T_2, T_3, T_h, F_x, and F_y:

$$
\begin{bmatrix}
\dfrac{d}{dt}\left(\dfrac{\partial \mathcal{L}}{\partial \dot{\theta}_2}\right) - \dfrac{\partial \mathcal{L}}{\partial \theta_2} \\[2ex]
\dfrac{d}{dt}\left(\dfrac{\partial \mathcal{L}}{\partial \dot{\theta}_3}\right) - \dfrac{\partial \mathcal{L}}{\partial \theta_3}
\end{bmatrix}
=
\begin{bmatrix}
-T_3 - F_x l_2 \sin\theta_2 + F_y l_2 \cos\theta_2 \\[1ex]
T_3 - T_h - F_x l_3 \sin\theta_3 + F_y l_3 \cos\theta_3
\end{bmatrix}
\tag{5.9}
$$

$$
\text{where } \mathcal{L} = \sum_{i=2}^{3} \frac{1}{2} m_i(\dot{x}_i^2 + \dot{y}_i^2) + \frac{1}{2} I_i \dot{\theta}_i^2 - \sum_{i=2}^{3} m_i g y_i
$$

16
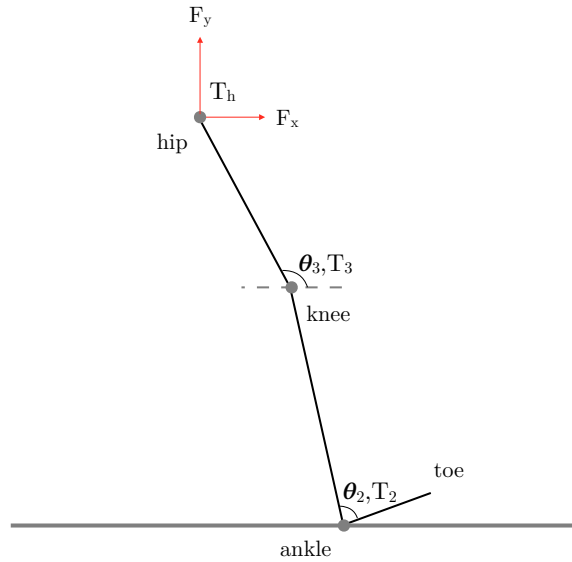
Figure 5-3: Schematic of the Heel Model, showing torque and angle notation for each joint.

5.3 Input

Literature data of a healthy pediatric gait profile was found and used as raw data for the both the Heel and Toe Models [19]. Figures 5-4 and 5-5 show the angles and torques, respectively, of each joint during the stance phase of a healthy 9 year old gait.
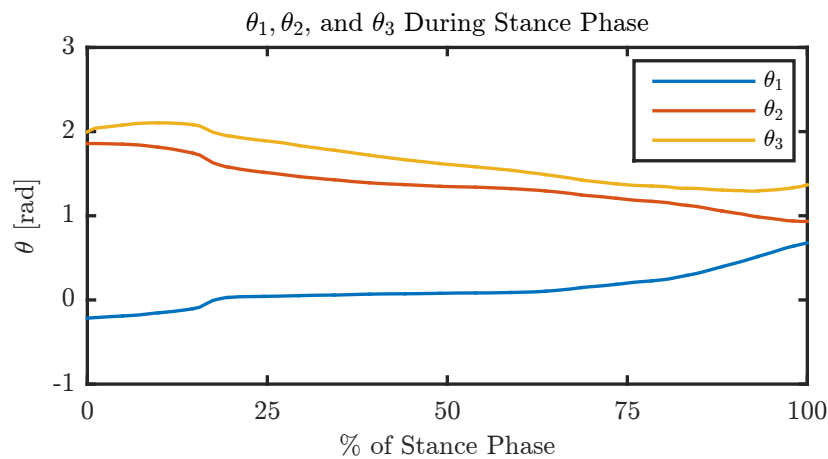
Figure 5-4: Joint angles during stance phase of healthy 9 year old gait.

In addition, anthropometric data corresponding to an average 9 year old child

17
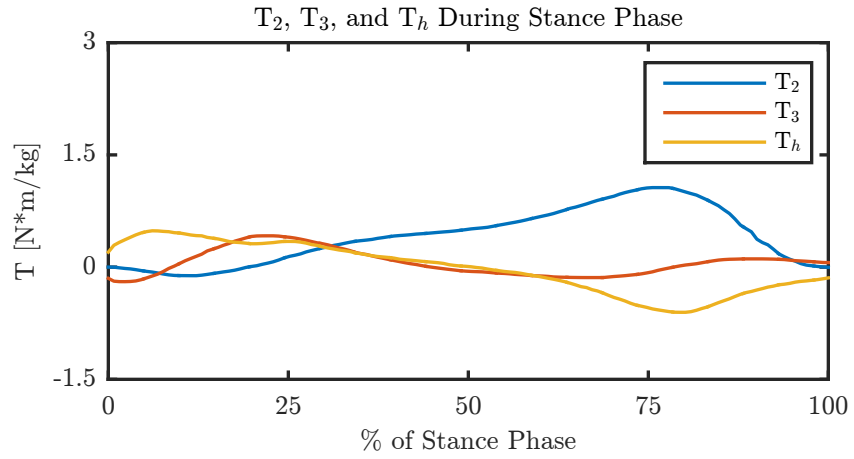
Figure 5-5: Joint torques during stance phase of healthy 9 year old gait.

was used [14]. Table 5.1 summarizes this data. The Center of Mass was defined as the distance from segment's center of mass to segment's distal end. The Moment of Inertia was defined around the segment's center of mass.

Limb	Parameter	Value
Foot	Mass	0.599 kg
	Length	0.219 m
	Center of Mass	0.113 m
	Moment of Inertia	0.0005 kg*m^2
Shank	Mass	1.90 kg
	Length	0.357 m
	Center of Mass	0.209 m
	Moment of Inertia	0.0150 kg*m^2
Thigh	Mass	4.58 kg
	Length	0.318 m
	Center of Mass	0.171 m
	Moment of Inertia	0.0360 kg*m^2

Table 5.1: Anthropometric data for a healthy 9 year old.

5.4   Model Execution and Results

5.4.1   9 Year Old Model

Using data from section 5.3 as input to both the Heel and Toe Models, F_x and F_y were solved for. In the Heel Model, F_x and F_y were the two unknown variables, whereas in the Toe Model, F_x, F_y, and T_1 were the three required unknowns. Figure 5-6 shows the computed F_x and F_y for the entire stance phase, after the results from the Heel and Toe Models were combined. Note that the transition between the two models occurs at around 18% of the stance phase, which corresponds to the time point at

which $\theta_1 = 0$.
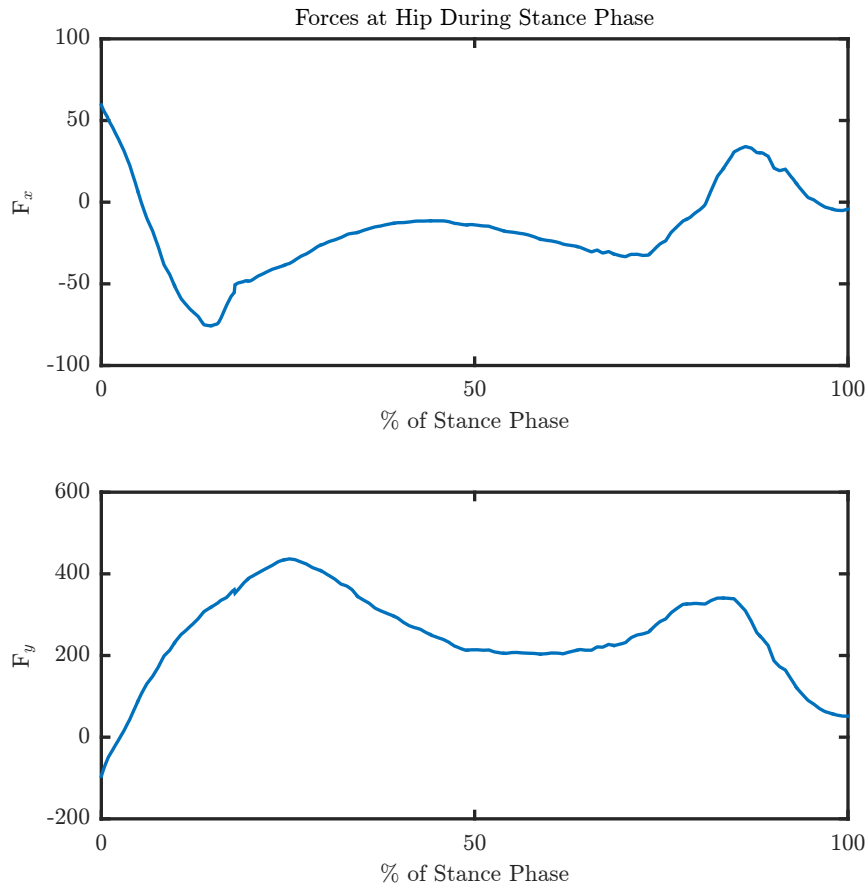
Figure 5-6: Derived horizontal and vertical forces acting on the hip joint throughout the stance phase (9 Year Old).

Subsequently, the derived values of F_x and F_y were fed back into the model in order to derive the kinematics of each segment throughout the gait cycle.

As expected, the angles derived from the model matched the joint angles shown in Figure 5-4, which were initially inputed into the model. The correlation coefficients between the derived angles and literature values were 0.9995 (θ_1), 0.9999 (θ_2), and 0.9997 (θ_3).This verification demonstrated the model's internal consistency and allowed the use of the model to predict the kinematics of gait at different ages.

5.4.2   7 and 11 Year Old Model

It has been custom in the field of biomechanics to scale joint torques by mass—this has been demonstrated in [14]. The masses of average 7, 9 and 11 year old children are 33.4 kg, 40.2 kg, and 46.4 kg, respectively [14]. This data was used to scale the initially used joint torques, which were based on a 9 year old. Furthermore, anthropometric data for an average healthy 7 year old and 11 year old child were gathered, and is listed in Table 5.2.

Limb	Parameter	7 Y.O.	11 Y.O.
Foot	Mass	0.458 kg	0.691 kg
	Length	0.203 m	0.242 m
	Center of Mass	0.105 m	0.126 m
	Moment of Inertia	0.0005 kg*m^2	0.0015 kg*m^2
Shank	Mass	1.54 kg	2.24 kg
	Length	0.331 m	0.395 m
	Center of Mass	0.194 m	0.231 m
	Moment of Inertia	0.0100 kg*m^2	0.0230 kg*m^2
Thigh	Mass	3.67 kg	5.43 kg
	Length	0.296 m	0.352 m
	Center of Mass	0.159 m	0.190 m
	Moment of Inertia	0.0250 kg*m^2	0.0560 kg*m^2

Table 5.2: Anthropometric data for a healthy 7 and 11 year old.

Using the data from Table 5.2 and the scaled joint torques, the MATLAB code was run again to calculate the joint angles for a 7 and 11 year old child during stance phase. Similar to the 9 year old case, the results from the Heel and Toe Models were combined, with the transition between the two models occuring at roughly 18% of the stance phase. Figure 5-7 is an overlay plot of the gait pattern during stance phase of children of all three ages groups.

The results demonstrate that while the joint torques change significantly as a child
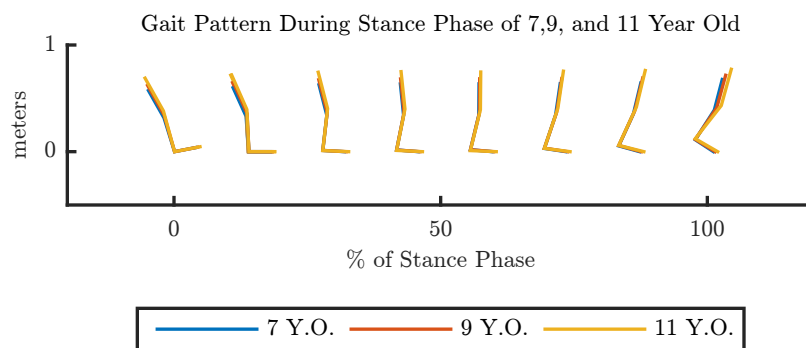
Figure 5-7: Derived stance phase gait pattern of 7, 9 and 11 year olds.

grows, the kinematics of the gait pattern remain largely consistent. This conclusion does not come as a surprise, since observable human gait is not noticeably different from person to person.

Chapter 6

Device Modeling

6.1 Overview

After a model for healthy pediatric gait at three ages (7, 9, and 11 years old) had been developed and validated, the model was modified to incorporate the replacement of the ankle joint with a prosthesis. As discussed in Section 3.1, the ankle is the simplest joint to replace, since a trans-tibial amputation does not affect proximal joints. This model, however, is scalable enough to model replacing additional proximal joints, as is necessary in trans-femoral amputations, for example.

The objective was to replace the torque at the ankle (generated from muscle contractions) in the healthy human model with torque generated from a spring element. A damping element was integrated to smooth the torque output.

Figure 6-1 shows both the biological angle and torque of the ankle during stance phase (specifically, during the time when the toe is in contact with the ground). We can ignore the heel contact portion of the stance phase because the prosthesis will not be producing any torque during this period. During this time, the ankle angle profile of the prosthesis will match the biological profile.

The figure demonstrates a roughly opposite relationship between angle and torque, where the torque produced by the ankle increases as the relative angle between the shank and foot decreases. A crucial feature of the prosthesis must be that the spring system matches this biological relationship between torque and angle.
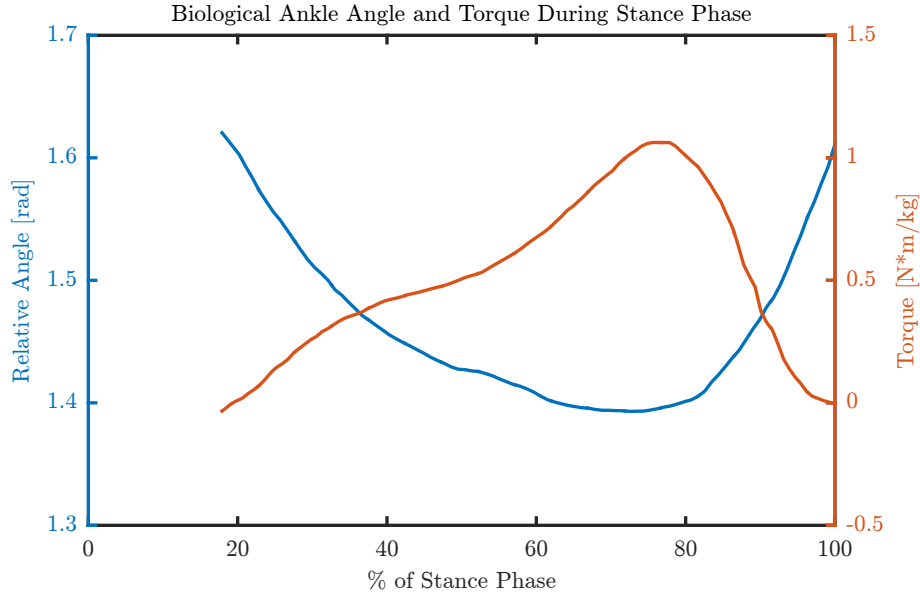
Figure 6-1: Relative ankle angle (between shank and foot) and torque during toe contact portion of stance phase of healthy 9 year olds.

6.2   Design Options

Multiple methods of configuring the spring and damper system were explored and evaluated. The variations on designs included changing the number of springs, orientation of the spring(s) with respect to the damper, as well as when each spring in a given design engaged.

6.2.1   Spring Damper Aligned

The first design is shown in Figure 6-2. Both the spring and the damper are anchored to the shank and foot, a certain distance away from the joint. Both the spring and the damper remain parallel to each other. The spring is oriented in a manner such that when the ankle angle decreases, the energy stored by the spring increases, similar to the behavior seen in Figure 6-1.

6.2.2   Spring Damper Offset

The next design was similar to the aligned design, but in this case, the spring and damper are not parallel. Figure 6-3 depicts the design. Similarly in this design, the
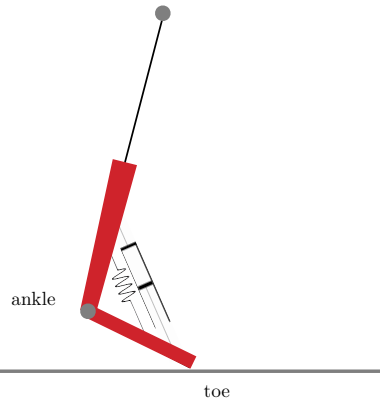
Figure 6-2: Spring damper aligned design.

torque generated by the spring increases as the ankle angle decreases.
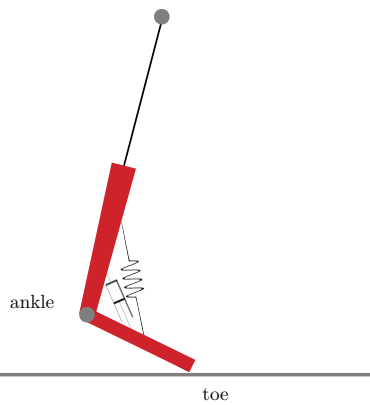
Figure 6-3: Spring damper offset design.

6.2.3 Double Spring

Next, a spring was added to the previous offset design. This new spring was mounted to the rear of the foot and was positioned in opposition to the initial spring. Figure 6-4 shows this design.

6.2.4 Variable Spring

Figure 6-1 shows that while the ankle angle and torque largely behave opposite to one another, there is a period between roughly 60% and 70% of the stance phase
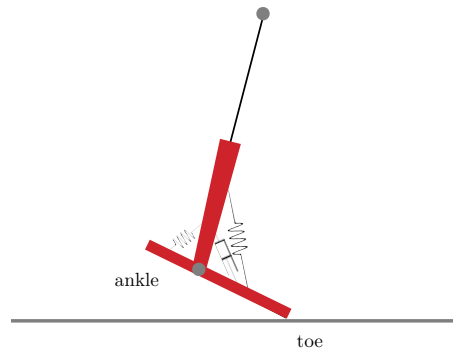
Figure 6-4: Double spring design.

when the torque continues to increase while the angle remains largely constant. In order to provide the ankle with additional torque only when the ankle has reached a threshold angle, an additional toe spring was added to the offset design. One end of a rod was mounted on a pivot to the shank, as shown in Figure 6-5. The other end is constrained to travel parallel and coincident to the foot.

(a) Ankle angle is greater than threshold angle. Toe spring not activated by the rod.

(b) Ankle angle is less than threshold angle. Toe spring is compressed by the distal end of the rod.
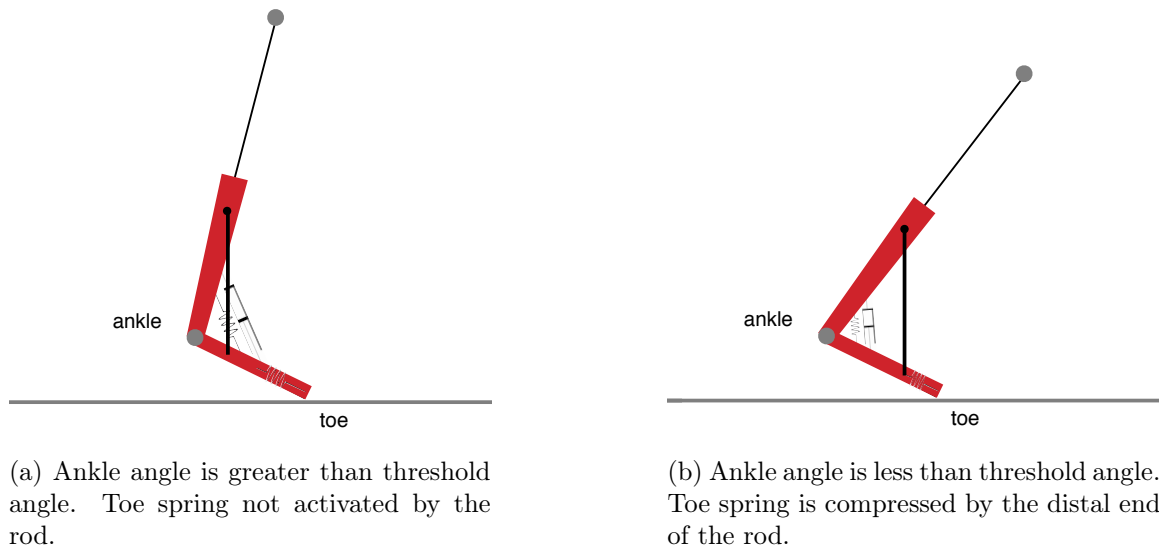
Figure 6-5: Variable spring design.

When the ankle angle is greater than the threshold angle (Figure 6-5a), the distal end of the bar is not in contact with the tow spring. When the angle decreases below the threshold (Figure 6-5b), the distal end of the rod travels distally along the foot and comes into contact with the toe spring, thus compressing the spring and

26

generating additional torque.

6.3   Modeling Spring/Damper System

In order to understand how the various prosthetic ankle designs would affect the gait pattern of a child, the following modifications to the initial MATLAB model were made:

1. An expression for the force exerted by the spring and damper system, with respect to the current joint angle as well as the current change in the angle (velocity), was derived.

2. The torque exerted by the spring and damper system, using the force previously determined, was calculated.

3. As outlined in Section 5.4.1, the derived values of F_x, F_y, joint torques and joint angle velocities at each time step were used to calculate the joint angles at the next time step (using **ode45**). Note that the literature values of T_2— the biological ankle torque—were not used. Rather, T_2 was recalculated, as described in step 2, every time step.

6.3.1   Optimization

Each of the designs presented in Section 6.2 had multiple associated parameters (ie. spring anchor location on shank, spring constant, damping coefficient, etc.). Table 6.1 lists all the free variables associated with each design. The "anchor" variable refers to the location at which the element is anchored relative to the ankle joint. For example, "damper shank anchor" represents the distance between the anchor point of the damper on the shank and the ankle joint.

   An optimization script in MATLAB was built in order to determine, for each design option, the values of associated free variables that produced the best torque profile. The cost function—minimizing the absolute difference between the prosthesis

Spring Damper Aligned	Spring Damper Offset
damping coefficient	damping coefficient
spring constant	damper shank anchor
spring resting length	damper foot anchor
spring/damper shank anchor	spring constant
spring/damper foot anchor	spring resting length
	spring shank anchor
	spring foot anchor

Double Spring	Variable Spring
damping coefficient	damping coefficient
damper shank anchor	ankle spring constant
damper foot anchor	ankle spring resting length
spring 1 constant	ankle spring/damper shank anchor
spring 1 resting length	ankle spring/damper foot anchor
spring 1 shank anchor	toe spring constant
spring 1 foot anchor	toe spring foot position
spring 2 constant	rod length
spring 2 resting length	rod shank anchor
spring 2 shank anchor	
spring 2 foot anchor	

Table 6.1: List of free variables associated with each spring/damper system design.

torque and the biological torque over the entire toe contact was—used to determine the best torque profile was described as follows:

$$\min \sum_t |T_{biological} - T_{model}|$$

Due to the number of free variables in each design option, some constraints were added, in order to reduce the solution space of the optimization program and speed up the process. These constraints were based off of design specifications listed in Section 3.1, anthropometric constraints from Tables 5.1 and 5.2, and torque considerations from Figure 6-1.

- Shank anchor point not to exceed maximum height of prosthesis (0.18 m).

- Foot anchor point not to exceed minimum length of foot (0.2 m).

- Figure 6-1 shows that the torque at the beginning and end of toe contact phase is close to 0. At these times, the corresponding ankle angle is around 1.62 rad. Thus, the absolute difference between the spring resting length and the distance between the spring anchor point on the shank and foot must not be greater than 5% when the ankle angle is 1.62 rad, to ensure close to 0 torque is applied at the beginning and end of toe contact (spring is nearly or fully relaxed).

6.3.2 Model Results

After running the optimization on all four designs, the optimal free variables were used to determine the torques generated in each design. As discussed at the beginning of Section 6.3, the revised MATLAB model was rerun to determine the new gait profiles generated as a result of each design. Figure 6-6 shows the torques generated by each prosthesis design, as well as the biological ankle torque.

Ankle Torque Outputs
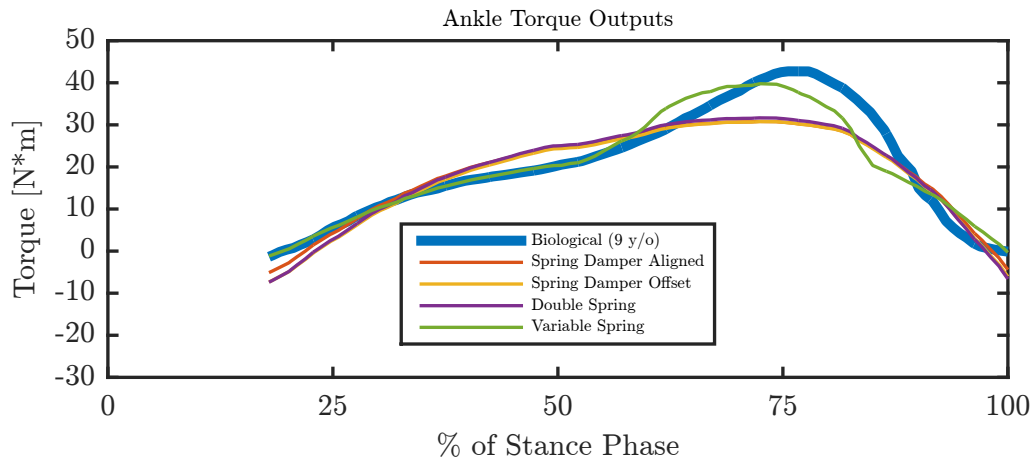
Figure 6-6: Torque delivered by biological ankle and all prosthesis designs during toe contact portion of stance phase.

Figure 6-7 shows the difference between the derived gait of a 9 year old child with the variable spring ankle prosthesis compared to biological gait. Note that between 0 and 18% of stance phase, the prosthesis gait pattern matches the biological pattern, as discussed in Section 6.1.

Unlike the other three designs, the variable spring prosthesis closely matched the biological torque profile up to around 60% of stance phase. The variable spring design
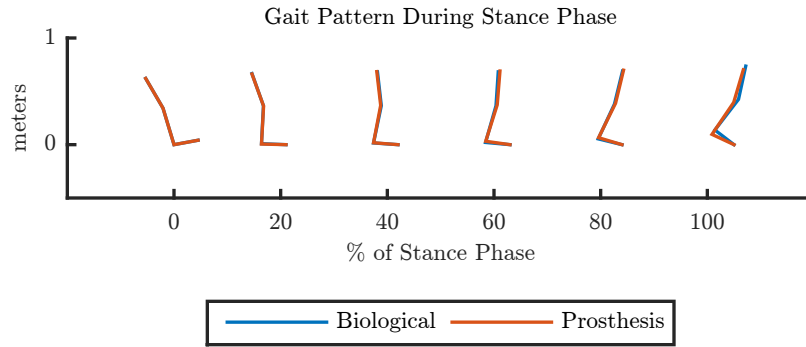
Figure 6-7: Derived gait pattern of 9 year old with variable spring ankle prosthesis.

also performed better during the latter portion of stance phase, providing more torque than the remaining design. This was due to the toe spring feature, which stores and releases additional energy only after the ankle angle decreases below a threshold angle.

6.4   Finalized Design Parameters

After the variable spring design was determined to be the most optimal of the four designs, the optimal values of the free variables were recorded, in order to inform the mechanical design of the device. Since nine independent free variables were associated with this specific design, some variables were constrained to specific values, in order to ease the designing of the device and material procurement. The constraints were as follows:

- Ankle spring resting length was constrained to be 3.5, 4, 4.5, 5, or 5.5 inches (to make purchasing springs easier)

- Ankle spring/damper anchors on the shank at 0.1 m proximal from ankle joint (approximately half the height of the device)

- Rod anchors on the shank at 0.1 m proximal from ankle joint (to utilize the same attachment point as the spring/damper in order to simplify design)

- Rod length is constrained to 0.15 m (given 0.1 m anchor point, 0.15 m rod length results in approximately 45 degree resting position angle)

After the constraints were set, the optimization was run again and the following finalized design parameters were generated:

Parameter	7 Y.O.	9 Y.O.	11 Y.O.
Ankle Spring Resting Length [m]	0.127	0.127	0.127
Ankle Spring/Damper Shank Anchor [m]	0.1	0.1	0.1
Rod Length [m]	0.15	0.15	0.15
Rod Shank Anchor [m]	0.1	0.1	0.1
Ankle Spring Constant [kN/m]	23.97	28.78	33.21
Damping Coefficient [N*s/m]	350	350	350
Ankle Spring/Damper Foot Anchor [m]	0.0746	0.0746	0.0746
Toe Spring Constant [kN/m]	222.7	268.8	310.3
Toe Spring Foot Position [m]	0.114	0.114	0.114

Table 6.2: Finalized design parameters for all ages. Bold parameters indicate values derived from optimization (unconstrained).

Chapter 7

Device Design

Based on the optimized device parameters for the variable spring design, listed in Table 6.2, a prototype of the ankle prosthesis was designed. This chapter describes the design process for each of the core components (spring, damper, adjusting mechanism) as well as for the final overall assembly. To summarize, the key design features for the variable spring design are as follows:

- Main ankle spring joining shank and foot

- Ankle damper joining shank and foot

- Secondary toe spring, only to be activated when ankle angle decreases past specific threshold

- Bar mechanism to be constrained by a pivot joint on the shank and a linear sliding joint on the foot and to be used to activated toe spring

7.1 Spring Design Options (Preliminary)

Given the device's requirement for two spring systems, multiple types of springs were evaluated: standard compression spring, torsional spring, elastic rope spring, air spring, leaf spring, magnetic spring, and disc spring. The following subsections

describe each design in depth as well as evaluates the appropriateness of each type for implementation into each of the two spring systems.

7.1.1 Standard Compression Spring

Using a standard compression spring as a means of storing and releasing energy is a simple way of meeting the requires spring constant. Compression springs with constants within the range of what is required can easily be obtained, and are affordable as well. In order to provide the necessary spring constants, however, these springs will need to be composed of metal and will likely be sizable (approximately an inch in diameter), which may add to the weight and size of the system. Despite these drawbacks, the fact that compression springs are common and readily available make easily replaceable and an attractive choice.

7.1.2 Torsional Spring

Similar to standard compression springs, torsional springs are also readily available and affordable. Because the ankle functions as a pivot joint, incorporating a torsional spring—where the radial axis of the spring is co-linear with the ankle joint's axis of rotation—may in fact reduce the size of the spring system, compared to a standard compression spring.

Since the prosthesis modeling in MATLAB was performed based on a linear spring, the model was modified to instead include a torsional spring at the ankle. The resulting spring constant requirement for a torsional spring was in the range of approximately 110 N*m/rad. The torsional spring with the largest available spring constant given the size constraints of the prosthesis had a constant of only around 0.1 N*m/rad. Selecting this design option would required a large number of springs combined in parallel in order to achieve the necessary effective spring constant.

7.1.3 Elastic Rope Spring

The elastic rope spring concept involves leveraging the elasticity of rubber tubing in order to store and release energy. Since literature data on the spring-like behavior of rubber tubing was unreliable, load vs extension tests were performed on three types of rubber tubing (thin, medium and thick as seen in Figure 7-1) in order to determine both whether a linear spring-like regime exists and whether the effective spring constant is sufficient to meet the design requirements. Figure 7-2 shows the results of the load vs extension tests, performed on an INSTRON.

Figure 7-1: Thin, medium and thick rubber tubing (dimensions in cm).
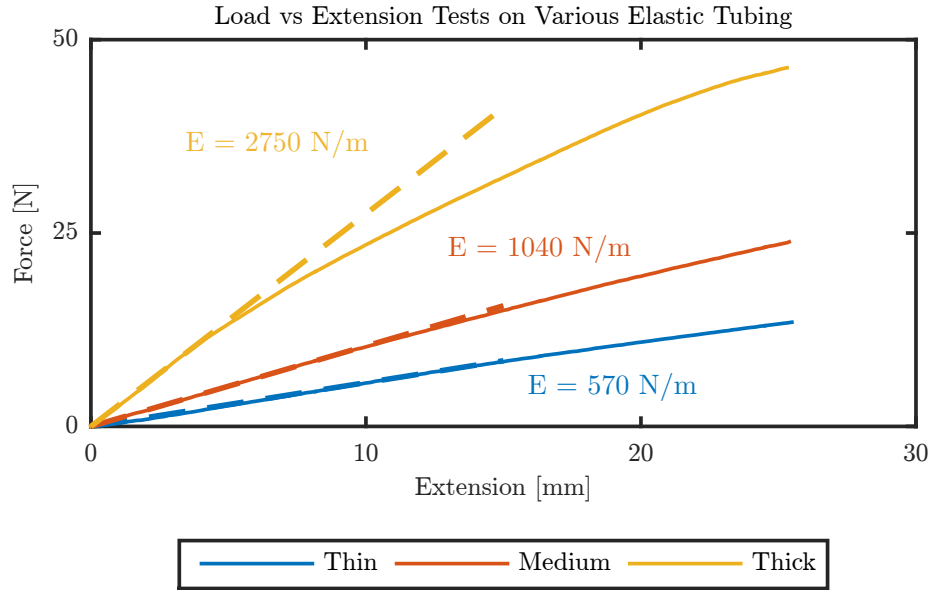
Figure 7-2: Load vs extention tests on three types of elastic tubing. Hashed line represents extrapolation of linear elastic region.

As the maximum displacement requirement of the ankle spring during the stance phase is approximately 10 mm, the INSTRON test was conducted to a maximum extension of 25 mm. The results show that while each of the rubber tubing displays a linear regime, characterized by Young's Moduli of 570 N/m, 1040 N/m, and 2750 N/m for the thin, medium and thick tubing, respectively. Given these results, in order to achieve the required spring constant for the ankle spring, at least 10 thick tubes (or 30 medium tubes or 60 thin tubes), need to be joined in parallel. If the thick tubes were to be bundled in a cylindrical collection, the cross-sectional diameter of this bundle would be at least 60 mm.

7.1.4 Air Spring

Another concept that was evaluated was a piston-cylinder system, where the compression of air by the piston would result in a linear spring-like behavior. In order to determine the feasibility of such a system, calculations were made to approximate the dimensions of the piston-cylinder system necessary to generate the forces required of the spring. Equation 7.1 describes the conservation of force, which was used to

determine the cross-sectional area of the piston necessary to produce a force of 300 N, which is the approximate magnitude of the force generated at maximum compression of both the ankle and toe springs. This value (300 N) was calculated using a spring constant of 30,000 N/m and change in length at maximum compression of 0.01 m for the ankle spring, and a spring constant of 300,000 N/m and change in length at maximum compression of 0.001 m for the toe spring.

$$P_1 V_1 = P_2 V_2 \tag{7.1}$$

$$P_2 = P_1 \frac{L_1}{L_2}$$
$$F = (P_2 - P_1)A$$
$$= P_1 A \left(\frac{L_1}{L_2} - 1 \right)$$
$$A = \frac{F}{P_1 \left(\frac{L_1}{L_2} - 1 \right)}$$

With F as 300 N, P as 101,325 Pa (atmospheric pressure), $\frac{L_1}{L_2}$ as $\frac{0.1m}{0.09m}$ for the ankle spring and $\frac{L_1}{L_2}$ as $\frac{0.05m}{0.049m}$ for the toe spring, the necessary surface area for the piston in the ankle spring and toe spring, respectively, would be 0.026 m^2 and 0.15 m^2. Assuming a piston with a circular cross-section, the diameter of the cross-section would be 0.18 m and 0.44 m for the ankle piston and toe piston, respectively. Given the width of a human foot is far less than 0.18 m, this simple calculation demonstrates that solely due to size, an air spring would not be a feasible solution for either spring system.

7.1.5 Leaf Spring

The leaf spring concept consists of a simple cantilevered beam, constrained at one end and free at the other. As shown in Figure 7-3, a force applied at the free end results in a deflection of the beam and a reaction force proportional to the deflection. As such, the cantilever, or leaf spring, can be thought of as exhibiting a spring-like behavior.
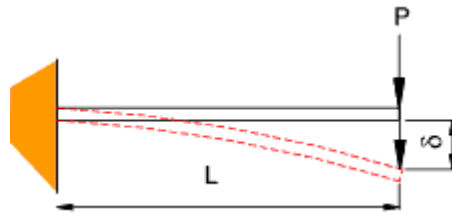
Figure 7-3: Cantilever leaf spring [20]

Equation 7.2 expresses the effective spring constant of the leaf spring system in terms of the Young's Modulus and dimensions of the beam.

$$k = \frac{Ebt^3}{4L^3} \tag{7.2}$$

For the purposes of determining the feasibility of using a leaf spring, some approximations were made. The beam was assumed to be made of carbon-fiber (E = 0.8 GPa) [21], a thickness (t) of 0.005 m, and a width (b) of 0.05 m. Given the required effective spring constants of 30,000 N/m and 300,000 N/m at the ankle and toe springs, respectively, the required length of the cantilever beam would be 0.15 m and 0.07 m.

7.1.6 Magnetic Spring

The manufacturer Polymagnet is vendor of magnets that exhibit spring-like properties (Figure 7-4). At a distance, two of these magnets attract, but when brought close

together beyond a threshold, the two magnets repel one another. Figure 7-5 is from
Polymagnet's product specification sheet, showing a graph of the spring-like behavior.

Figure 7-4: Spring magnet from Polymagnet [22].
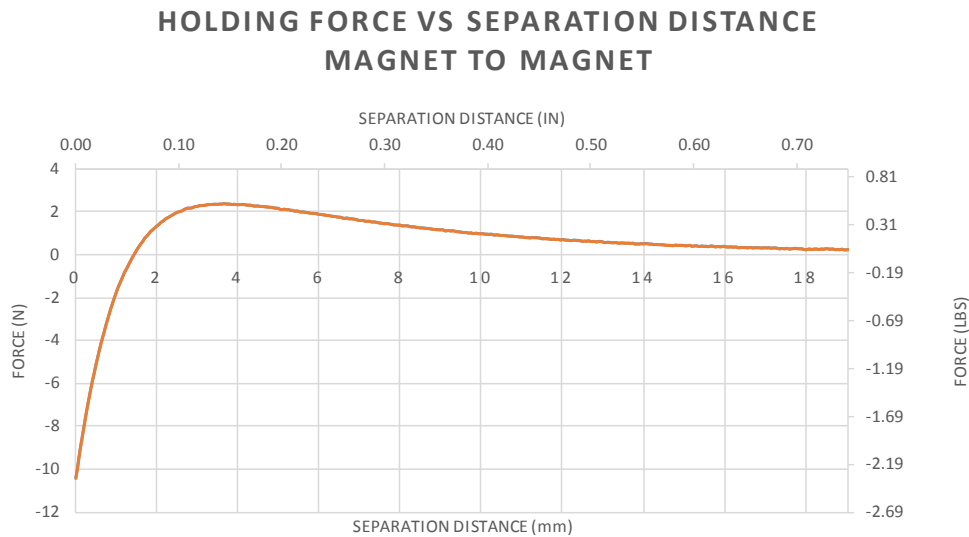
Figure 7-5: Magnetic force of Spring-like Polymagnets at various separation distances
[22].

As we can see from Figure 7-5, the magnets exhibit an approximately linear be-
havior when the distance between them is less than approximately 1.5 mm. This
regime can be approximated by an effective spring constant of 6,700 N/m. Given this
approximation, in order to achieve the required ankle spring constant, at least five of
these magnet pairs are required.

Figure 7-6: Disc springs stacked (left) and individual schematic (right) [23].

7.1.7 Disc Spring

A disc spring (Figure 7-6), also known as a Belleville washer, is typically a metal convex disc supported on its edge that stores energy as a force is applied to its center.

Since this type of spring is best suited for small displacements, the design would be better suited for the toe spring. Using disc springs for the ankle spring system would require a large number of discs, which would add to both the cost and size of the device. The use of disc springs, even for the toe system, may be problematic, however, because the behavior of the discs have been shown to be non-linear [24].

7.1.8 Evaluation

The seven spring concepts were evaluated using the Pugh chart, shown in Table 7.1. Each of the concepts was evaluated in terms of its general criteria (durability, material cost, assembly cost, ease of assembly, user interaction, and replaceability), as well as criteria specific to the ankle or toe spring (accuracy and size). Durability referred to performance over repeated use. Material cost represented the cost of the spring, while assembly cost represented the cost of constructing a mechanism to accommodate the spring. Ease of assembly indicated the difficulty of designing a mechanism to accommodate the spring. Finally, user interaction and replaceability refer to the difficulty for parents to adjust the springs to change age setting and to

replace the spring mechanism if it were to break, respectively.

For a particular criterion, each design concept was assigned a score of -1, 0 or +1. The total score for a given spring concept at a particular location (air spring concept for the toe spring system) was determined by adding up the weighted sum of the criteria. Highest weights were assigned to cost and accuracy measures, followed by durability, size, ease of assembly, and user interaction.

		Standard Compression Spring	Torsional Spring	Elastic Rope Spring	Air Spring	Leaf Spring	Magnetic Spring	Disc Spring
2	Durability	1	1	0	0	1	1	1
3	Material Cost	1	0	1	-1	1	-1	0
3	Assembly Cost	0	0	1	-1	0	-1	-1
2	Ease of Assembly	1	0	1	0	1	0	1
2	User Interaction	0	0	1	-1	0	-1	0
1	Replaceability	1	0	1	-1	0	-1	-1
3	Ankle Spring Accuracy	1	1	-1	1	1	-1	-1
2	Ankle Spring Size	0	0	1	-1	-1	0	-1
3	Toe Spring Accuracy	1	1	-1	1	1	-1	0
2	Toe Spring Size	0	0	0	-1	1	-1	1
	Ankle Spring Total	**11**	**5**	**10**	**-8**	**8**	**-10**	**-5**
	Toe Spring Total	**11**	**5**	**8**	**-8**	**12**	**-12**	**2**

Table 7.1: Pugh chart of preliminary spring design concepts.

The results of the Pugh chart indicate that while the standard compression spring is clearly the best choice for the ankle spring system, both the compression spring and leaf spring are feasible design options for the toe spring. The compression spring's cost, precision, and ease of use make it an optimal option for the ankle spring, but the leaf spring's compactness and precision at small displacements improves the concept's suitability for the toe spring. In order to hone in on the most appropriate concept and design for the spring systems, further evaluation needed to be conducted.

7.2   Spring Design Options (Final)

Preliminary evaluation of spring designs, conducted in Section 7.1.8, concluded that a compression spring was most appropriate for the ankle spring, while a compression spring or a cantilever leaf spring were suitable for the toe spring. Based on these conclusions, more detailed designs for these options were constructed and evaluated.

Figure 7-7 shows the two designs for the ankle spring and three designs for the toe spring.
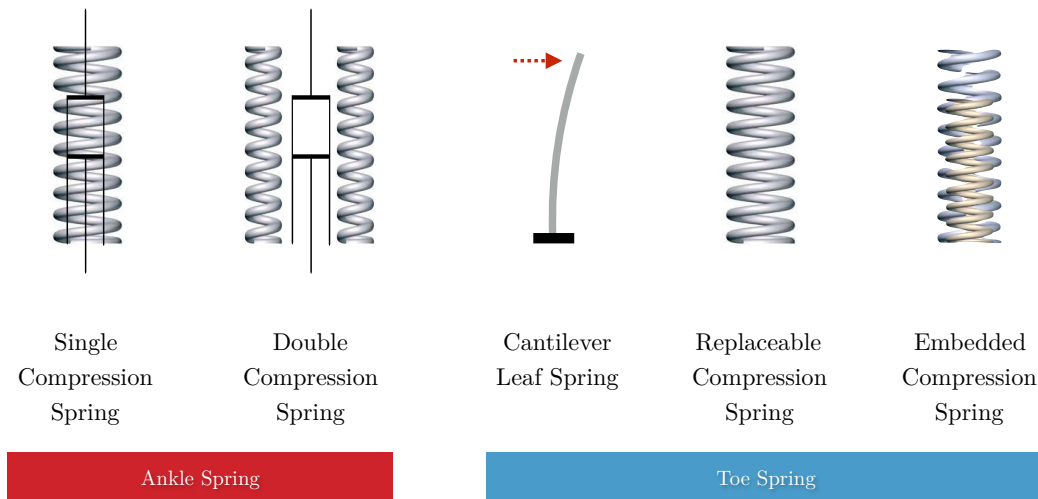
Figure 7-7: Designs for ankle spring (left) and toe spring (right).

7.2.1   Ankle Spring Options

The first ankle spring design involved a single compression spring configured coaxially with a single damper. The benefits of this design include small space requirement (since the damper is embedded within the spring cavity) as well as cost (only a single spring is required). As the spring constant requirement changes with age, only a single spring needs to be replaced. A limitation of this design, however, is that since the damper is fixed at both ends to the shank and foot, replacing the compression spring requires removing an anchor from one end of the damper.

An alternate ankle spring design attempted to eliminate the limitation of the

41

single spring design by placing two springs on either side of the damper. Replacing the springs as the patient ages would not require any interaction with the damper. The disadvantages of this design are both cost and size, since halving the spring constant requirement, particularly in the range of 30,000 N/m, does not significantly reduce the size or cost of springs.

7.2.2   Toe Spring Options

As previously mentioned, both a leaf and compression springs were suitable contenders for the toe spring system.

The leaf spring design, consisting of a simple cantilever beam constrained at one end and with force applied at the other end, was described in 7.1.5. The benefits of this design include its simplicity, ease of manufacturing, and low cost. The behavior of this cantilever, however, remains linear only with small deflections.

The replaceable compression spring design is similar to the single compression spring design presented as an option for the ankle spring. For the purposes of the toe spring, however, replacing the compression is less difficult since there is no coaxial damper. The toe system, however, needs to be significantly smaller, since the width of the foot at the toe is constrained to approximately 60 mm and the weight of the foot can be no greater than 0.5990 kg (Table 5.1).

Since the replacing of springs could be cumbersome, an alternate design (embedded compression spring) was envisioned, where additional smaller springs would be place coaxially and within a larger central spring. As the requirements for the toe spring constant increase with age, the additional embedded springs could be "activated" by pushing them forward and into contact with the plane upon which force is applied. Disadvantages of this design, however, are its weight (since all springs, even inactive ones, are fixed on the foot) as well as cost of manufacturing the mechanism that activates and deactivates the embedded springs.

7.2.3   Evaluation

Similar to Section 7.1.8, the two ankle spring designs and three toe spring designs were using the Pugh chart, shown in Table 7.2. Each of the concepts was evaluated in terms of its ease of user interaction, size, weight, accuracy and cost. Again, each design concept was assigned a score of -1, 0 or +1 for each design criterion. The total score for a given spring concept was determined by adding up the weighted sum of the criteria. Highest weights were assigned to the ability for a user to easily interact and adapt the springs as well as to size.

		Ankle Spring		Toe Spring		
		Single Compression Spring	Double Compression Spring	Cantilever Leaf Spring	Replaceable Compression Spring	Embedded Compression Spring
3	User Interaction	0	1	1	0	1
3	Size	1	0	1	1	0
2	Weight	1	0	1	0	-1
1	Accuracy	1	1	0	1	1
2	Cost	1	0	1	1	0
	Total	**8**	**4**	**10**	**6**	**2**

Table 7.2: Pugh chart of final spring design concepts.

The evaluation concluded that a single compression spring, with a damper placed coaxially, for the ankle spring as well as a cantilever leaf spring for the toe system would be the optimal combination.

7.3   Damper Selection

The damper in the variable spring design has a required damping coefficient of 350 N*s/m. Airpot Corporation is a manufacturer of high-precision, low friction dashpots with adjustable damping coefficients. Based on the required coefficient, the 2KS95 dashpot model, seen in Figure 7-8, was selected. This model was the lowest profile dashpot whose coefficient range still included the required 350 N*s/m. The datasheet for this dashpot can be found in Figure B-1.

Figure 7-8: 2KS95 dashpot by Airpot [25].

7.4   Final Design

7.4.1   Ankle Spring

Based on the conclusion that a single compression spring, which could be replaced as a pediatric amputee grew, would provide the optimal design for the ankle spring system, three springs—one for each age group—were sought that matched the required specification. Table 7.3 shows both the requirements for the ankle spring for each age group, as well as the parameters for each spring that was determined to most closely match the requirements. All springs were sourced from Lee Spring.

Requirements	7 Y.O.	9 Y.O.	11 Y.O.
Resting Length [m]	0.127	0.127	0.127
Spring Constant [kN/m]	23.97	28.78	33.21

Spring Part No.	LHC 192N 07M	LHC 207N 06S	LHC 207N 06M
Resting Length [m]	0.127	0.127	0.127
Spring Constant [kN/m]	24.5	29.7	34.1
Outer Diameter [in]	1.25	1.25	1.25
Rod Diameter [in]	0.804	0.775	0.775

Table 7.3: Requirements for ankle spring as well as specification of springs chosen from Lee Spring [26].

Since Lee Spring does not carry any springs that perfectly match the spring constants required, the springs selected represent the closest matched to what the modeling deemed to be optimal. Using the spring constants of the available springs, the

prosthesis MATLAB model was run again to determine if the difference between the available and ideal spring constant would affect the torque output of the ankle. Figure 7-9 shows the torque output from a prosthesis with the optimal spring constant compared to that from a prosthesis using the available Lee Spring in the 9 year old case. The correlation coefficient between these two outputs is 1.00, which confirms that the difference between the actual and ideal spring constant is not significant. A similar conclusion was made for the 7 and 11 year old cases.
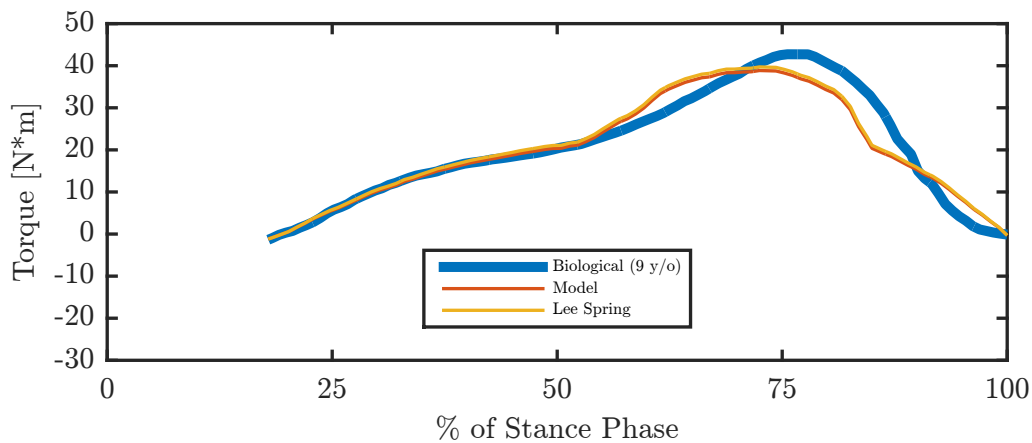
Figure 7-9: Torque delivered by prosthesis with optimal spring and prosthesis with Lee Spring LHC 207N 06M (9 year old child).

7.4.2 Ankle Spring/Damper Assembly

The ankle spring/damper assembly, which includes the Lee Springs described in Section 7.4.1 and the 2KS95 dashpot described in Section 7.3, serves three purposes: to attach the ankle spring to the shank and foot, to attach the damper to the shank and foot, and to allow the easy replacement of the spring once a pediatric amputee grows.

To achieve these functions, two core components were designed: an upper spring holder and a lower spring holder. The upper spring holder latches onto a quarter-inch rod, which is fixed to the shank, while the lower spring holder hinges to a quarter-inch rod, constrained to the foot. Both holders sandwich the spring, containing it. When the ankle angle decreases, the separation between the two holders decrease,

thus compressing the spring. Engineering drawings for the upper and lower spring holders are show in Figures B-2, B-3, and B-4.

The two holders also act to anchor the dashpot. One end of the dashpot cylinder is threaded (3/8-32) and screws into a tapped hole on the lower spring holder. The piston, which slides within the cylinder, is fixed to a threaded rod (4-40). The upper spring holder consists of a 4-40 screw that is constrained in line with the dashpot's rod. A threaded standoff provides the medium by which the 4-40 screw of the upper spring holder is connected to the rod/piston of the dashpot.

Figure 7-10 shows an exploded view of the ankle spring/damper assembly, which contains the upper and lower spring holders, the spring, the dashpot, and the threaded standoff.
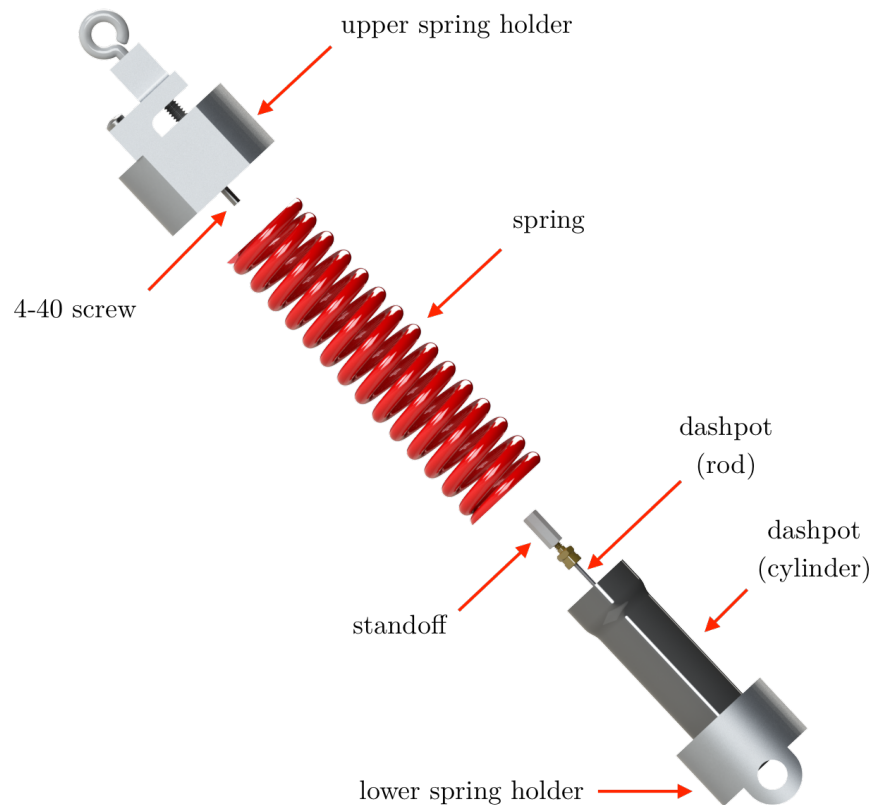
Figure 7-10: Exploded view of ankle spring/damper assembly.

Figure 7-11 shows the ankle spring/damper assembly attached to the prosthesis

shank and foot via quarter-inch rods.
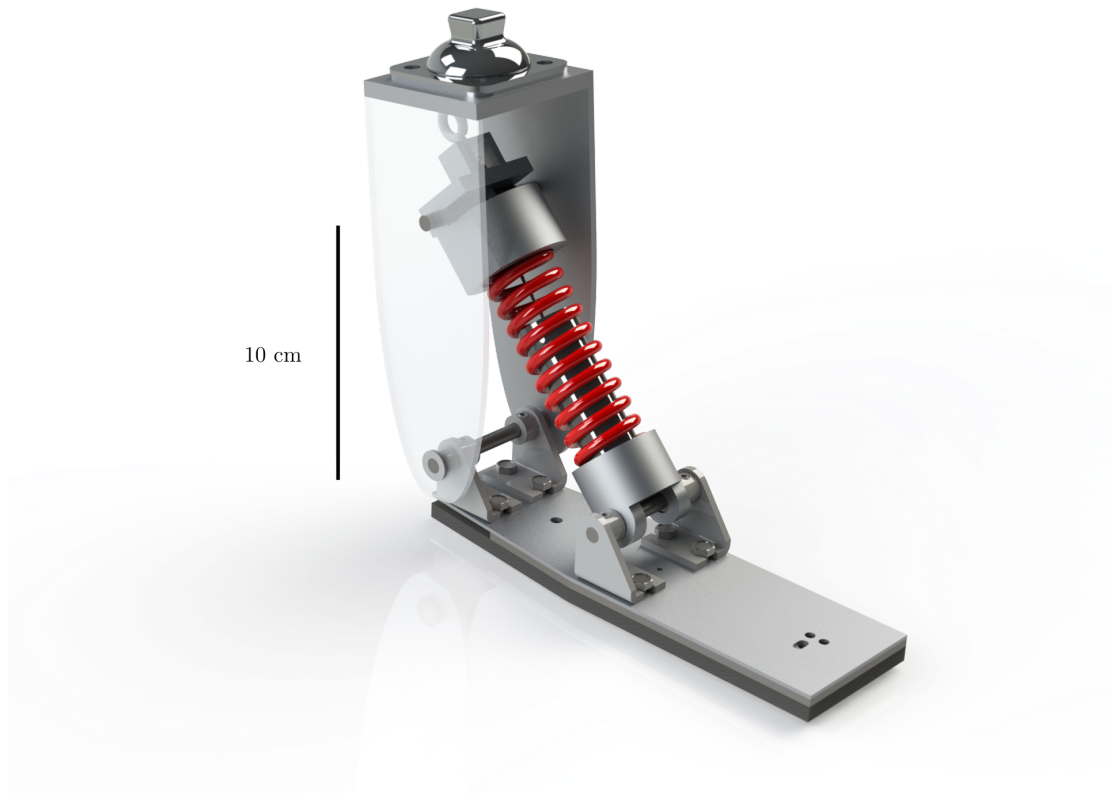
Figure 7-11: Ankle spring/damper assembly anchored to prosthesis shank and foot.

The design of the upper spring holder also allows for the easy replacement of the spring, when needed. The upper spring holder consists of a spring-loaded pin (in the form of an eyebolt), which keeps the holder latched to the quarter-inch shank rod. The spring-loaded feature ensures the eyebolt remains tightly in place, securing the upper spring holder to the shank rod. When the eyebolt is pulled, as shown in Figure 7-12 the holder is free to slide off the rod, thus freeing the ankle spring/damper assembly from the shank.

(a) Resting position. (b) Eyebolt pin pulled.
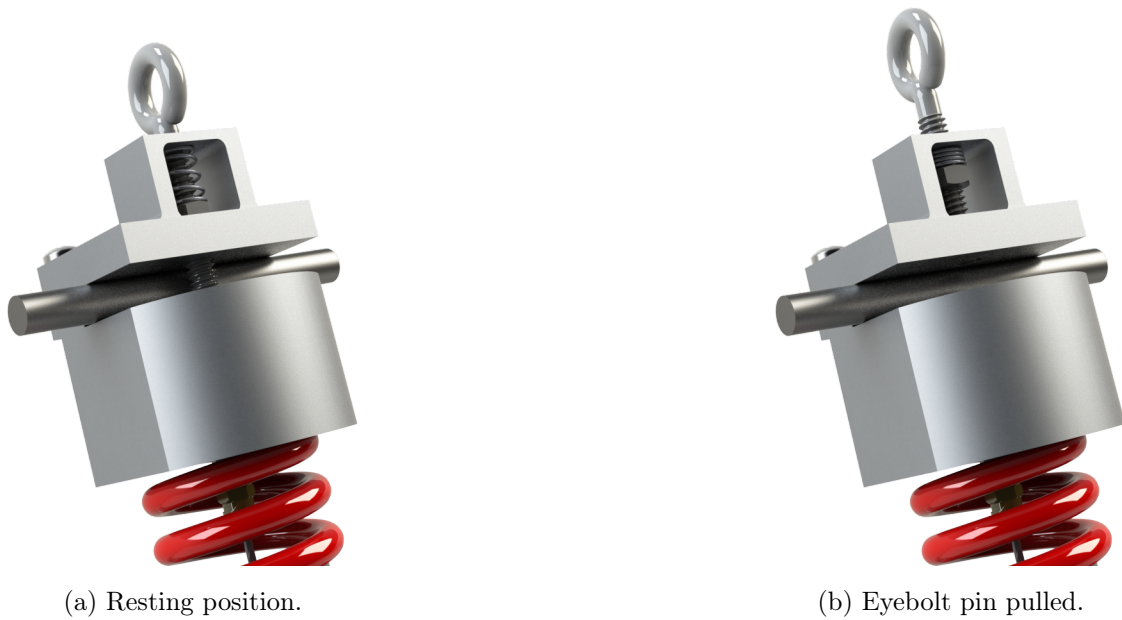
Figure 7-12: Upper spring holder release mechanism.

Once this occurs, the upper spring holder may be disconnected from the dashpot by unscrewing the standoff, thus allowing the spring to be removed from the assembly and replaced. This three step process of replacing the ankle spring (pull eyebolt pin, free ankle spring/damper assembly from shank, and disconnect upper spring holder) is summarized in Figure 7-13.
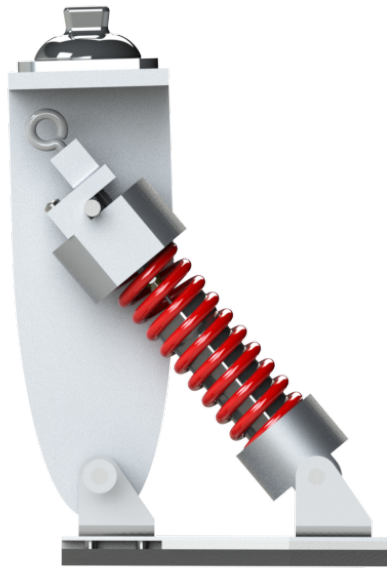
(a) Resting position.
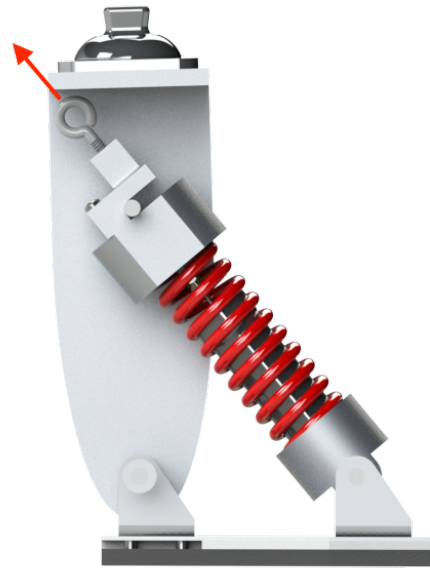
(b) Pull eyebolt pin.
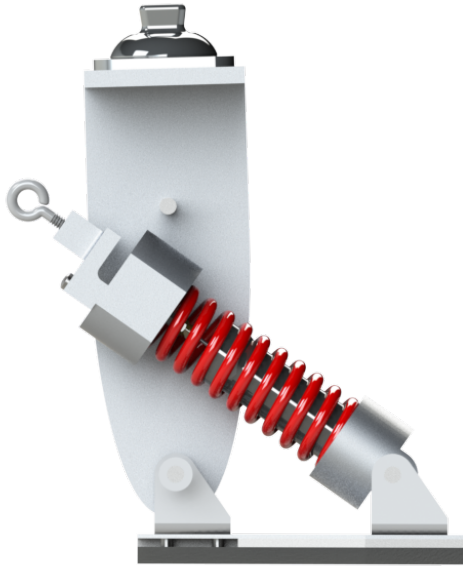
(c) Detach assembly from shank rod.
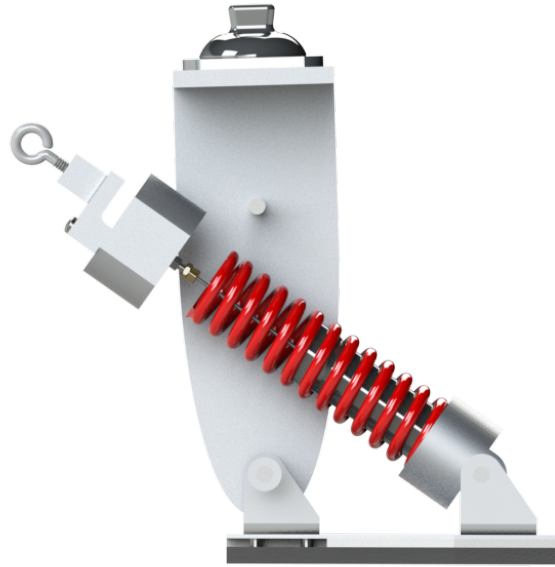
(d) Remove upper spring holder and replace spring.

Figure 7-13: Three-step process to replace ankle spring.

7.4.3   Toe Spring

The design for the toe spring cantilever system involved a beam, which deflects in the transverse plane of the foot when the ankle rod applies a force on the beam. In order to provide stability, two rods were used, one on each side of the foot. Since each rod was designed to apply force to the cantilever system, the optimal design involved anchoring the center of the beam in the center of the foot, while allowing each free end of the beam to act as a contact point for the ankle rod. In effect, the anchor allowed a single beam to act as two cantilevers. A overhead schematic of the toe spring cantilever system is shown in Figure 7-14.
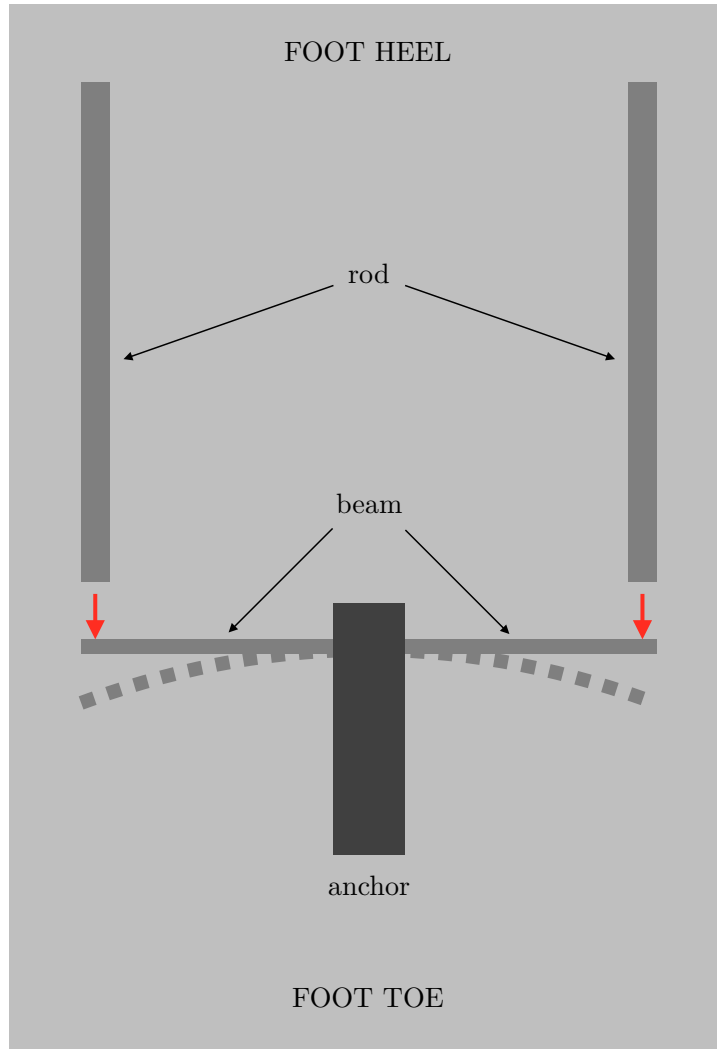
Figure 7-14: Overhead schematic of toe cantilever spring mechanism, showing point of contact between rods and cantilever beam (red arrows) as well as deflected beam (hashed line).

Since the effective spring constant of the cantilever spring needed to be tunable, an adjusting mechanism was built into the design of the anchor. The central anchor, shown in Figure 7-14, was designed as two separate pieces: a fixed component that remained fix to the foot, thus securing the cantilever beam in place as well as an adjustable component that could slide laterally. While the fixed anchor maintains the length of one of the cantilevers—thus keeping its spring constant fixed, the sliding mechanism was designed to reduce the effective length of the remaining cantilever, thereby increasing the effective spring constant. Figure 7-15 shows this adjustment

process.

(a) 7 year old position.

(b) 11 year old position (adjustable anchor moved to the left).
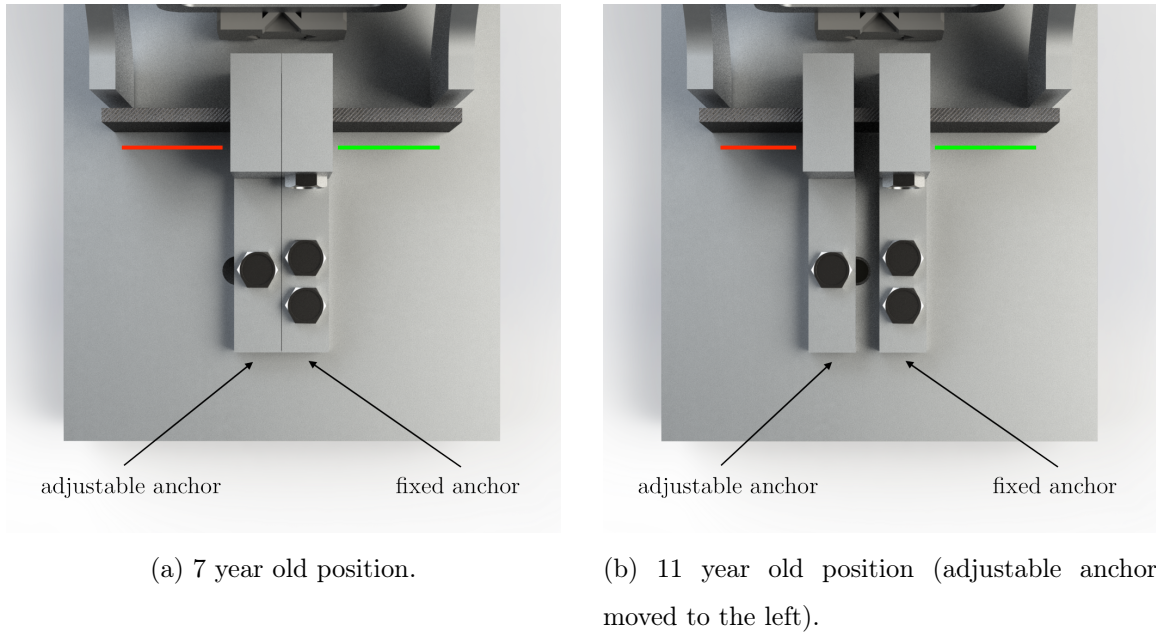
Figure 7-15: Overhead view of toe spring adjustment mechanism. Red and green line show effective length of adjustable and fixed cantilever, respectively.

Based on the conclusions from Section 6.4, the required spring constants for the cantilever toe spring were determined and are shown in Table 7.4.

Requirements	7 Y.O.	9 Y.O.	11 Y.O.
Spring Constant [kN/m]	222.7	268.8	310.3

Table 7.4: Required toe spring constants for each age setting.

Since the required spring constant increases with age, the adjustable anchor was designed to be moved further away from the fixed anchor with age. This implied that for the 7 year old case, both anchors would be touching and the lengths of both cantilevers would be equal. Based on these requirements, the necessary effective spring constant for cantilevers on the side of the fixed and adjustable anchors were determined and are shown in Table 7.5.

Spring Constant [kN/m]	7 Y.O.	9 Y.O.	11 Y.O.
Fixed Cantilever	111.4	111.4	111.4
Adjustable Cantilever	111.4	157.4	198.9

Table 7.5: Required toe spring constants for each cantilever (fixed and adjustable).

After the specification for the spring constants were determined, the next task was to select a material to use for the cantilever beam. The first requirement established for such a material was that the maximum stress achieved during deflection was at most a tenth of the material's yield strength (Safety Factor of 10). The two materials evaluated were Aluminum 6061 (E = 241 MPa, σ_{yield} = 240 MPa) and Carbon Fiber (E = 827 MPa, σ_{yield} = 600 MPa) [21][27].

For a given beam, the stress at a distance y from the neutral axis during bending can be expressed in terms of M, the bending moment and I the cross-sectional moment of inertia about the neutral axis:

$$\sigma = \frac{My}{I} \tag{7.3}$$

Given that

1. $M = k\delta L$ where k is the effective spring constant of the beam, δ is the deflection, and l is the length of the beam

2. L was expressed for in Equation 7.2

3. A beam with width b and thickness t has a moment of inertia of $\frac{bt^3}{12}$

4. The maximum stress in such a beam occurs when $y = t/2$

Equation 7.3 can be rewritten as:

$$\sigma_{max} = \frac{d}{t}\left(\frac{Ek^2}{4b^2}\right)^{1/3} \tag{7.4}$$

Based on this expression, the maximum bending stress was determined for beams of both Aluminum 6061 and Carbon Fiber at varying thicknesses (t), assuming: the beam width was 0.5 in, the maximum deflection was 2 mm, and the effective spring constant was 198.9 kN/m (required k in 11 year old case). Figure 7-16 shows the maximum stress at various thicknesses for both materials along with the yield strength of each material scaled down by a factor of 10.
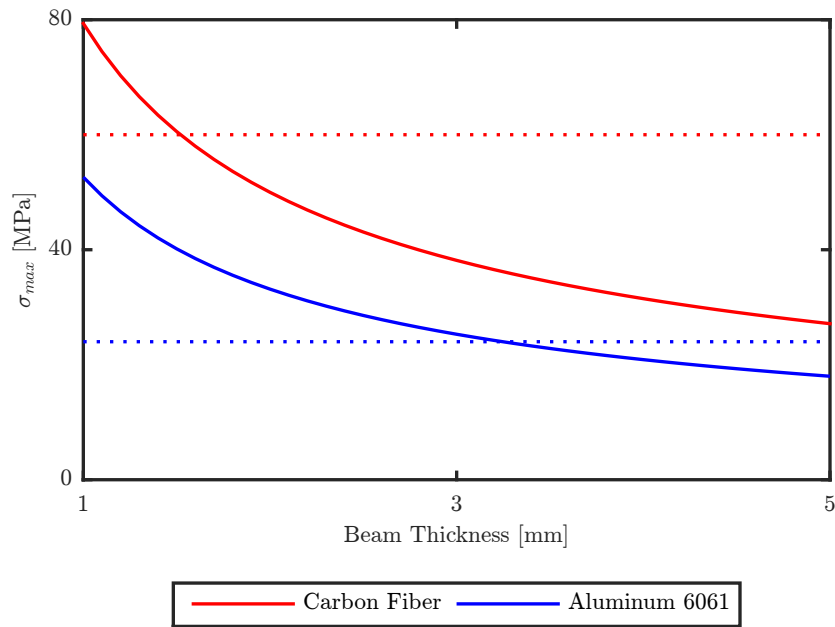
Figure 7-16: Maximum beam bending stress in various materials and material yield strength with a Safety Factor of 10 (dotted line).

The plot demonstrated that the maximum bending stress in a carbon fiber cantilever would only exceed the safety threshold when the beam is thinner than 1.5 mm, while the aluminum beam would do the same at less than 3.2 mm thickness. From this graph alone, it was determined that using carbon fiber as a material would allow a wider range of suitable beam thicknesses, whereas aluminum would be far more

constraining.

Given the requirement that the carbon fiber beam needed to be thicker than 1.5 mm, a few stock dimensions of carbon fiber beams from McMaster-Carr were evaluated. Since carbon fiber is relatively more difficult to machine and modify, it was assumed the stock thickness and width of the carbon fiber options would not be modified; only the length could be altered using a bandsaw. Furthermore, a constraint of 0.5 in (12.7 mm) was placed on the maximum width of the cantilever beam, in order to keep the toe spring system low profile. Thus, the three stock options that were evaluated had dimensions of: 1.78 mm x 11.1 mm, 2.33 mm x 5.58 mm, and 3.18 mm x 12.7 mm. Using Equation 7.1, the length of the adjustable cantilever was determined for each of the three stock carbon fiber options. Figure 7-17 shows the range of lengths required in order for each stock material to adjust from a 7 to 9 to 11 year old child as well as the maximum stress in the beam that would be generated as a result of these beam dimensions. A constraint was also set in order to ensure the maximum length of the cantilever did not exceed 20 mm. This was to ensure the combined length of the two cantilevers and two anchors did not exceed the width of the foot.

The plots demonstrated that the carbon fiber stock with thickness 1.78 mm was the only feasible option. The 2.33 mm thickness beam resulted in a maximum stress that exceeded the safety threshold, while the 3.18 mm beam required a cantilever length that—for the 7 and 9 year old cases—exceeded the allotted length. The finalized cantilever lengths are shown in Table 7.6.

Length [mm]	7 Y.O.	9 Y.O.	11 Y.O.
Fixed Cantilever	16.53	16.53	16.53
Adjustable Cantilever	16.53	14.73	13.62

Table 7.6: Required lengths of cantilevers (fixed and adjustable) for each age setting.

This implied that the adjustable anchor would need to move laterally by 2.91 mm
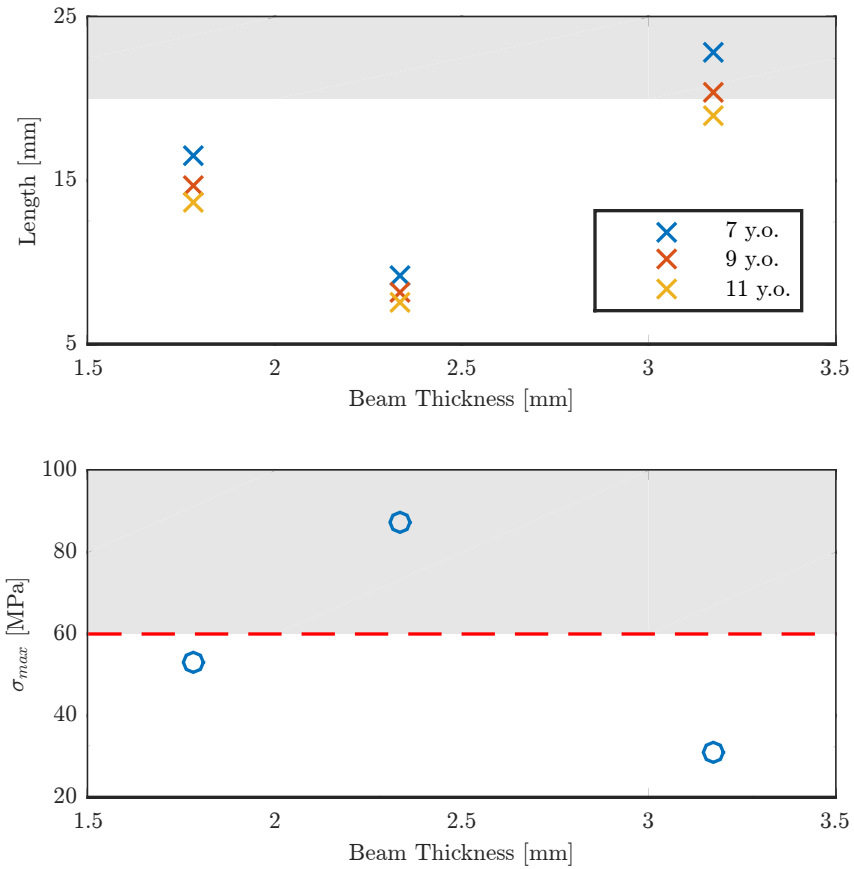
Figure 7-17: Required cantilever beam length for various stock carbon fiber options (top) and maximum stress corresponding to those cases (bottom). Yield strength, with a safety factor of 10, in dotted line; infeasibility regions in shaded grey.

in order to adjust the effective spring constant from the 7 year old setting ($k = 222.7$ kN/m) to the 11 year old one ($k = 310.3$ kN/m).

7.4.4 Toe Spring Assembly

In addition to the carbon fiber beam and anchors, the toe spring assembly also consisted of the ankle rods that applied a force on each cantilever when the ankle angle decrease beyond a threshold value.

First, the thickness of the rods were determined. Taking into consideration the maximum spring constant of the toe system is around 200 kN/m for a given cantilever (Table 7.5), each of the two rods needed to be designed such that they did not

buckle under load when the cantilever deflects by 5 mm. The resulting critical load requirement was 200 N (200 kN/m × 1 mm). The buckling equation (Equation 7.6) was used to determine the required thickness (t) of the rod, assuming a width (b) of 10 mm, length (L) of 0.15, composed of Aluminum 7075 (E = 70 GPa). A safety factor of 10 was incorporated (critical force F = 10000 N).

$$F = \frac{\pi^2 EI}{L^2} \tag{7.5}$$

$$
\begin{aligned}
F &= \frac{\pi^2 E b t^3}{12L^2} \\
t &= \left(\frac{12FL^2}{\pi^2 Eb}\right)^{\frac{1}{3}} \\
&= 2 \text{ mm}
\end{aligned}
$$

Thus, the width of each of the two rods was selected to be 1/8 in.

As determined in Section 6.4, the proximal ends of these rods (total length of 0.15 m) would hinge to the flank at a distance 0.1 m proximal from the ankle joint. The distal end of these rods would be connected to the foot through a linear sliding joint, thus constraining each rod's distal end to the plane of the foot. When the distal ends of the rods slide beyond a distance of 114.15 mm from the ankle joint, the rods will come into contact with the cantilevers.

In order to constrain the rods to the foot, a linear sleeve bearing and guide rail system were used. The guide rail was designed to screw to the foot. The sleeve bearing, which slides along the guide rail, was attached to a U-channel, which was used to connect to the distal ends of the ankle rods via a quarter inch horizontal rod. Figure 7-18 shows a rendering of the linear sleeve bearing system.
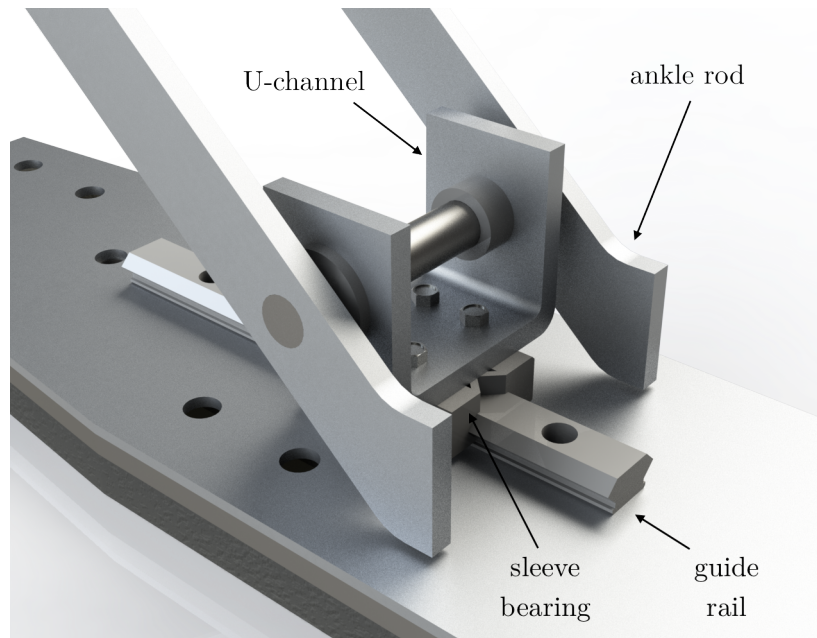
Figure 7-18: Rendering of sleeve bearing system, which constrains the distal end of the two ankle rods to the foot.

Figure 7-19 shows the entire toe spring assembly (both the ankle rods, linear bearing system, and toe cantilevers). At large ankle angles, the ankle rods are not in contact with the toe cantilevers. When the ankle angle decreases, the ankle rods move forward along the foot until, at a certain threshold angle, they come into contact with and engage the toe cantilever springs.

Figure 7-19: Toe spring assembly, showing toe cantilevers in resting position (left) and toe cantilevers engaged by ankle rods (right).

Also incorporated into the design of the toe spring assembly was the ability to change both the cantilever spring constant as well as the length of the foot in a single adjustment step. This was intended to improve the user-friendliness of the adjustment process, allowing parents to easily modify their child's prosthesis.
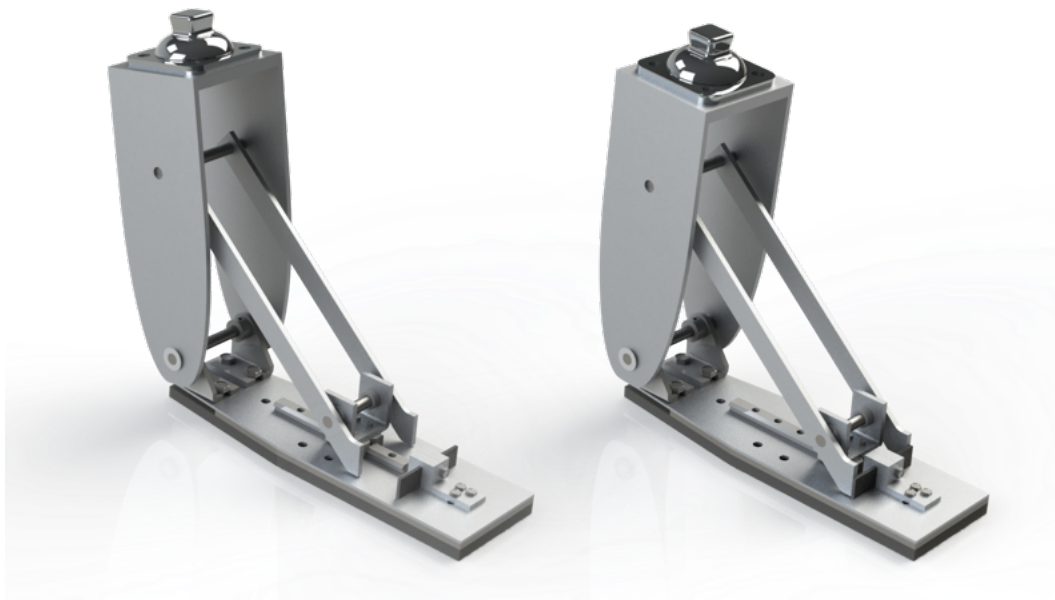
The prosthesis foot design consisted of two pieces, a thin upper piece that is directly hinged to the shank, as well as a thicker lower piece. The lower piece fixed to the upper piece with two bolts, one near the rear of the foot and one that passes through the adjustable anchor in the toe spring system. Unscrewing these bolts allow the forward and backward movement of the lower foot piece, in order to make the length of the foot longer as the child grows. These bolts could then be re-tightened to secure the new foot length (age) setting.

The holes in the lower foot piece were drilled such that the adjustable anchor could only be secured if its horizontal position (corresponding to a particular effective

cantilever length) matched with the correct overall length of the foot. For example, at the 7 year old setting, the adjustable anchor could only be secured if the anchor was in the initial position (touching the fixed anchor) and the lower foot piece was in the most retracted position. Only then would the securing bolt pass through all three pieces (the anchor and both foot pieces). Likewise, at the 11 year old setting, both the adjustable anchor needed to be displaced as far horizontally as possible (as seen in Figure 7-15) and the lower foot piece needed to be pulled as far out as possible in order for the bolt to be secured.

Figures 7-20 and 7-21 show the adjustment process between the 7 year old and the 9 year old settings.
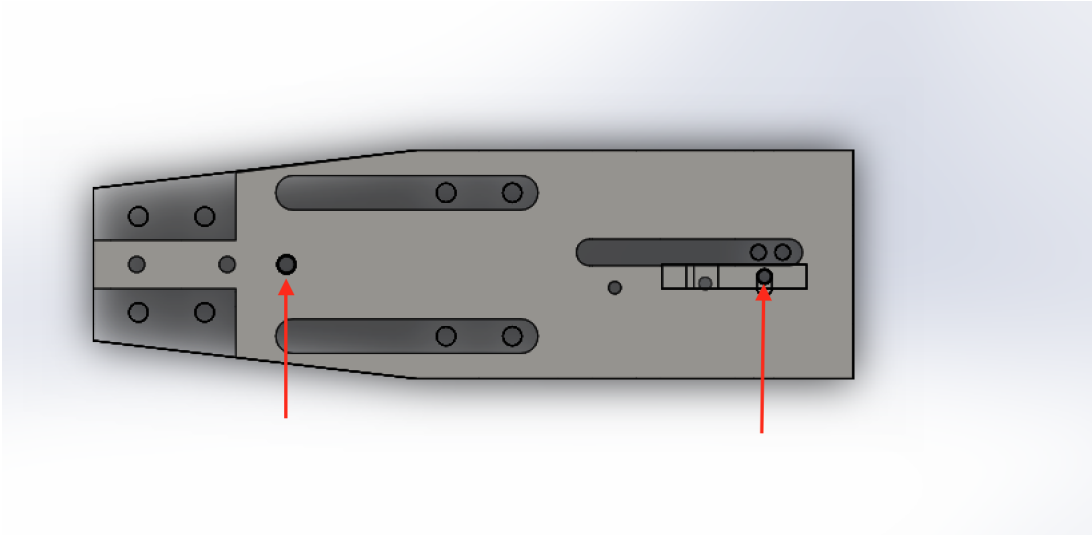
(a) 7 year old setting.
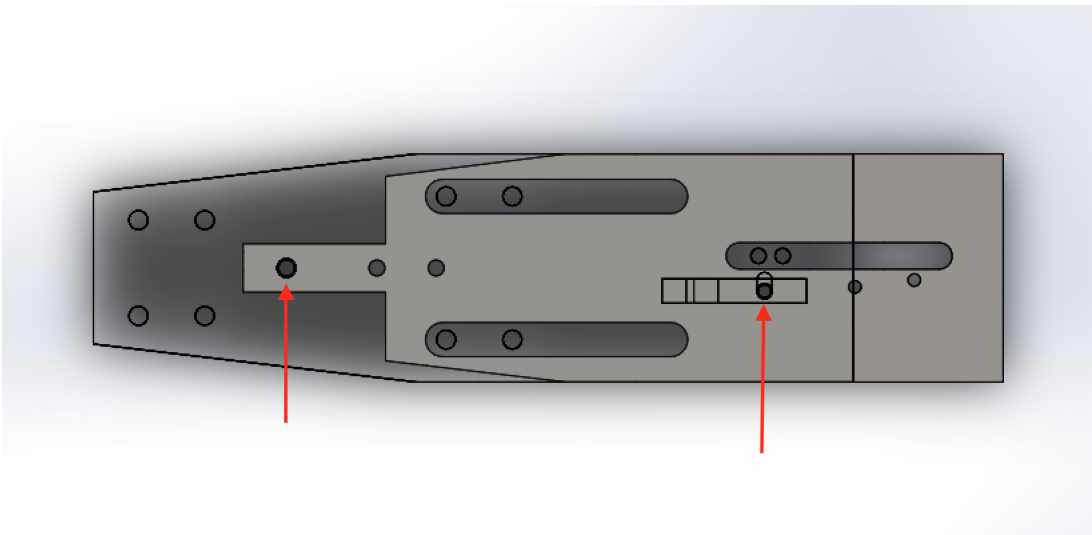
(b) 11 year old setting.

Figure 7-20: Overhead view of upper (transparent) and lower footplates, showing adjustment between 7 year old (a) and 11 year old (b) settings. Red arrows point to securing bolt hole locations.
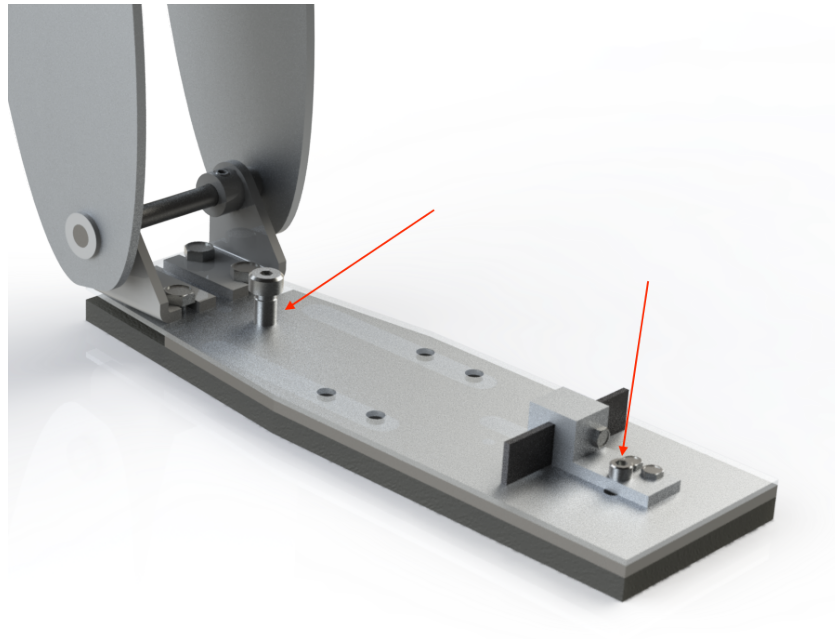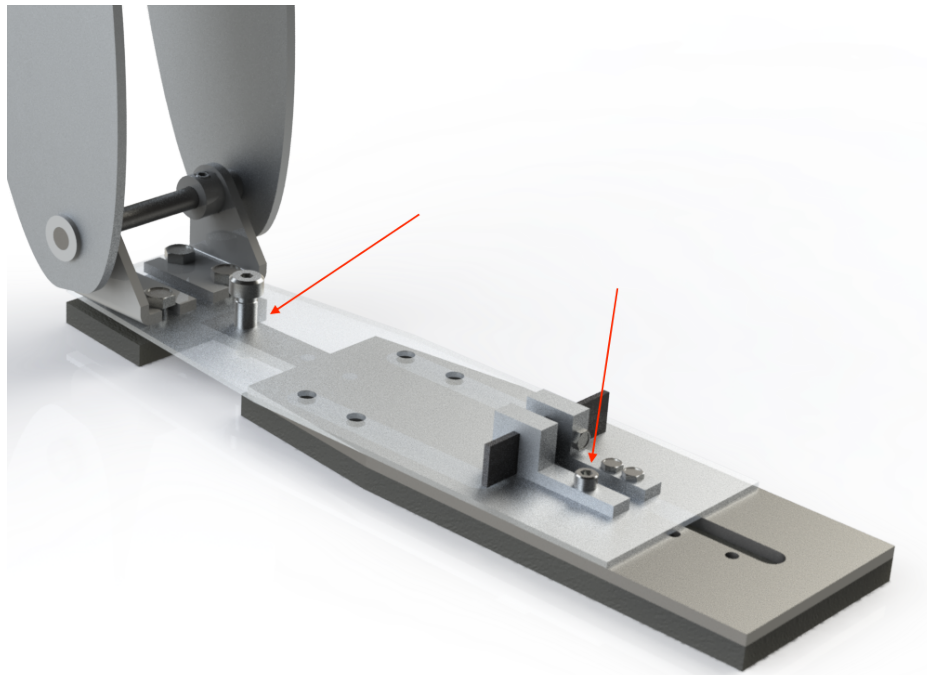
(a) 7 year old setting.

(b) 11 year old setting.

Figure 7-21: Perspective view of upper (transparent) and lower footplates, showing adjustment between 7 year old (a) and 11 year old (b) settings. Red arrows point to securing bolts.

7.4.5 Final Assembly

In addition to the two spring assemblies, additional pieces, including the shank, foot, and socket adapter were incorporated to provide structural and functional integrity. The function of the shank and foot was to secure and align the prosthesis, while the standard prosthetic adapter was incorporated to allow the attachment of a socket (beyond the scope of this project).

Figure 7-22 depicts the prosthesis in different colors, each corresponding to a different method of fabrication. Parts in blue were manufactured by waterjetting aluminum 7075, red parts were purchased as stock, and green parts were CNC milled.
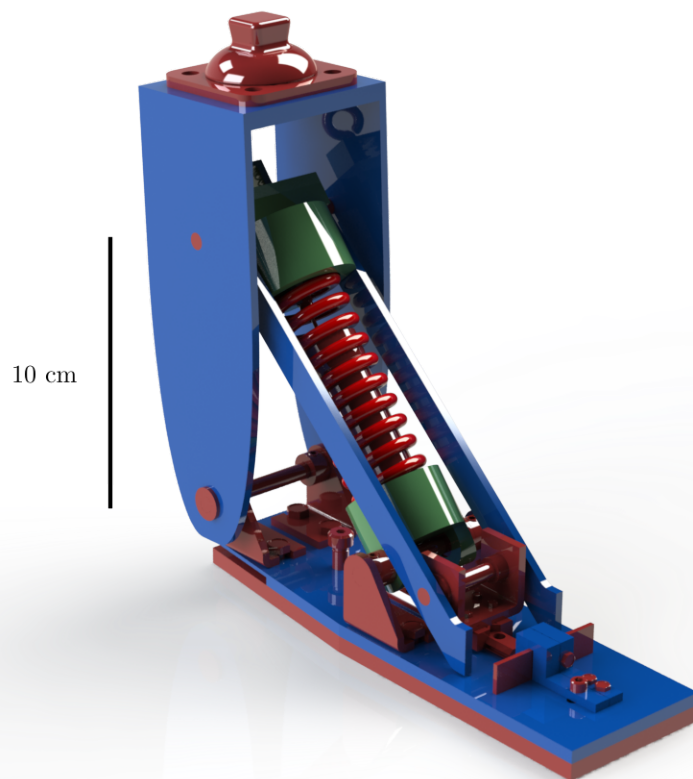

10 cm

Figure 7-22: Various manufacturing techniques used: waterjetting (blue), stock parts (red), and CNC milling (green).

Figure 7-23 shows a picture of the constructed prototype. A silicone foot was

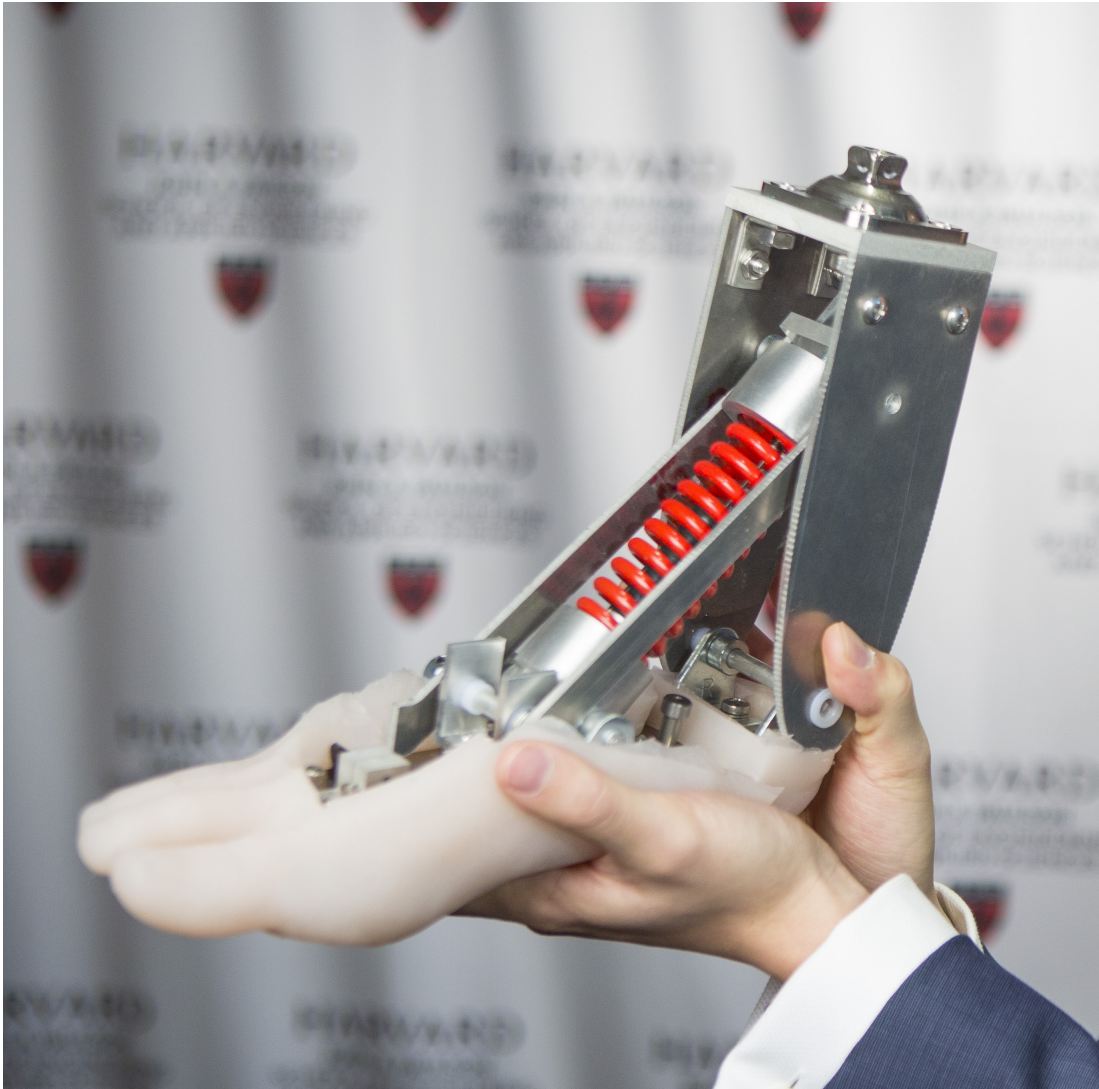molded and fitted to the foot plate for aesthetic purposes.

Figure 7-23: Final manufactured prototype.

Chapter 8

Device Evaluation

8.1 Experimental Setup

After the device was constructed, two forms of testing were conducted. The first test performed was static. The objective was to understand the torque generated by the ankle at various ankle angles and to compare these results to both the derived model and the biological data. The second test conducted was dynamic. Here, the objective was to characterize the damping properties of the device and again to compare the results to the model and biological data.

Both tests involved attaching an in-line load cell (iPecs Lab System 6 degrees of freedom load cell) to the prosthesis adapter in order to measure the torque generated at the ankle. The distal end of the load cell was screwed to the prosthesis, while a stainless steel rod was fixed to the proximal end of the load cell to act as a long lever arm. The prosthesis was then clamped to a tabletop via a securing plate in order to keep the footplate level. This clamping ensured the angle measurements (angle between the lever arm and the tabletop) would be accurate. Even though the load cell collects torque information at the location of the load cell, the device has a feature that enables extrapolation of torque at the ankle joint (20 cm distal to the load cell). Figure 8-1 shows the experimental setup.
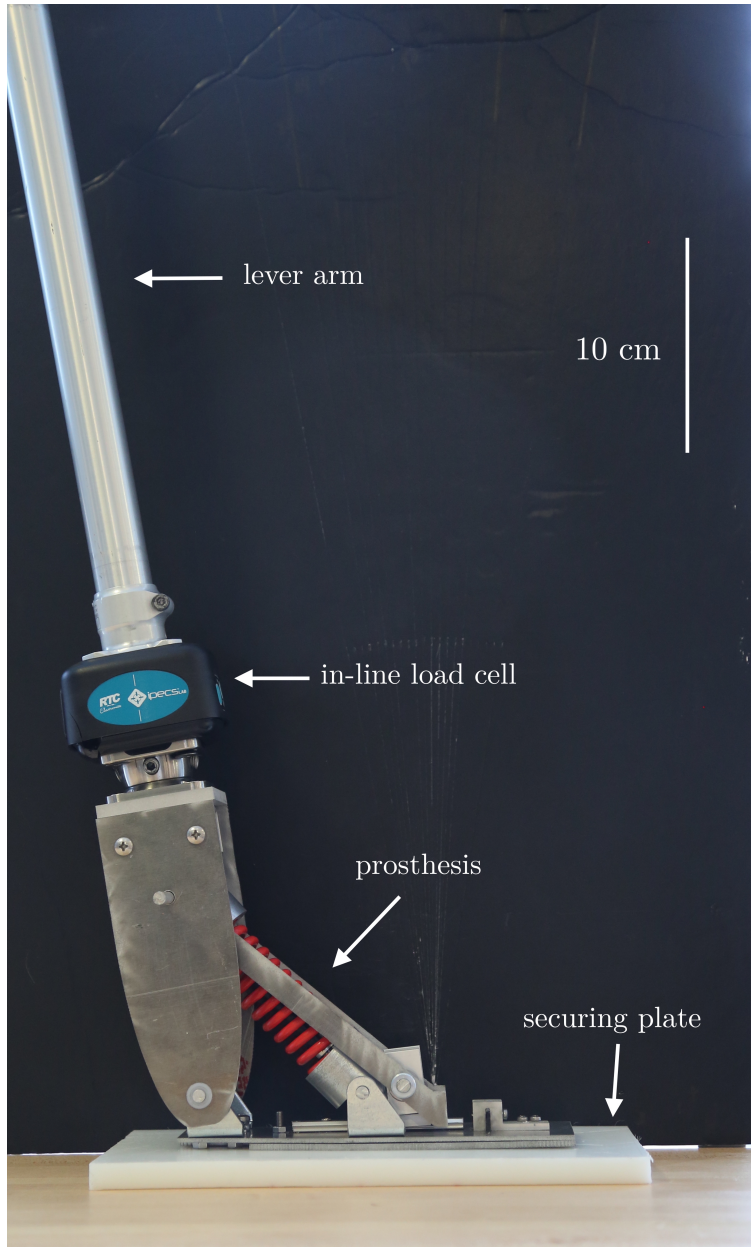
Figure 8-1: Photo of experimental setup showing prosthesis attached to load cell.

8.2 Static Testing

8.2.1 Protocol

By displacing pulling the lever arm, the ankle angle was manually displaced over a range of 12 degrees (from 92 to 80 degrees), which represents the approximate range of motion for a biological ankle during the gait cycle. The angle was decreased at an increment of 1 degree in a step function pattern, with each angle being held for 10 seconds. All three age settings were tested.

8.2.2 Data

Figures 8-2, 8-3, and 8-4 show the raw data collected from the iPecs load cell representing the ankle torque at various angles. At each setting (ages 7, 9, and 11), five trials were performed and recorded. At time 0, the ankle angle is at 92 degrees and the corresponding torque is 0. Every 10 seconds, thereafter, the ankle angle is reduced by 1 degree.

Figure 8-2: Prosthesis ankle torque at various angles (92 degrees at t = 0 s to 80 degrees at t = 120 s) at 7 year old setting. N = 5.
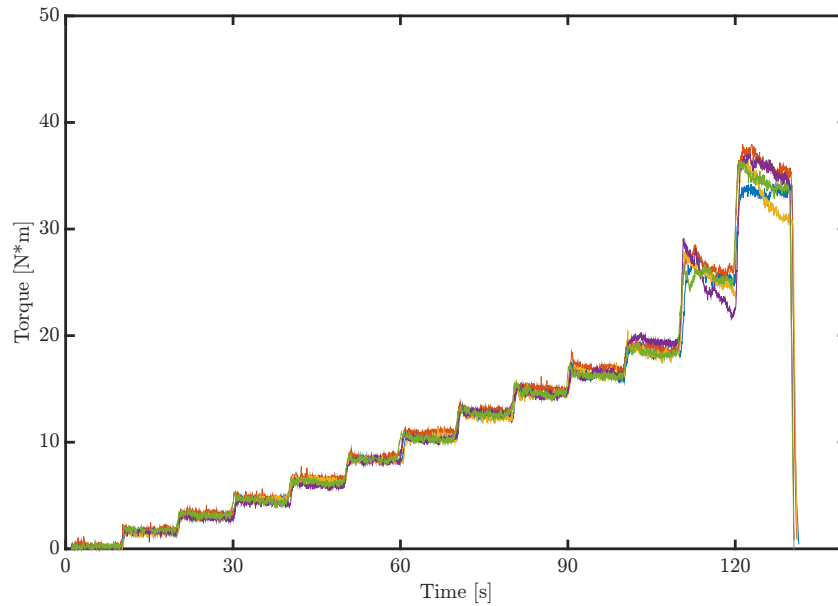
Figure 8-3: Prosthesis ankle torque at various angles (92 degrees at t = 0 s to 80 degrees at t = 120 s) at 9 year old setting. N = 5.
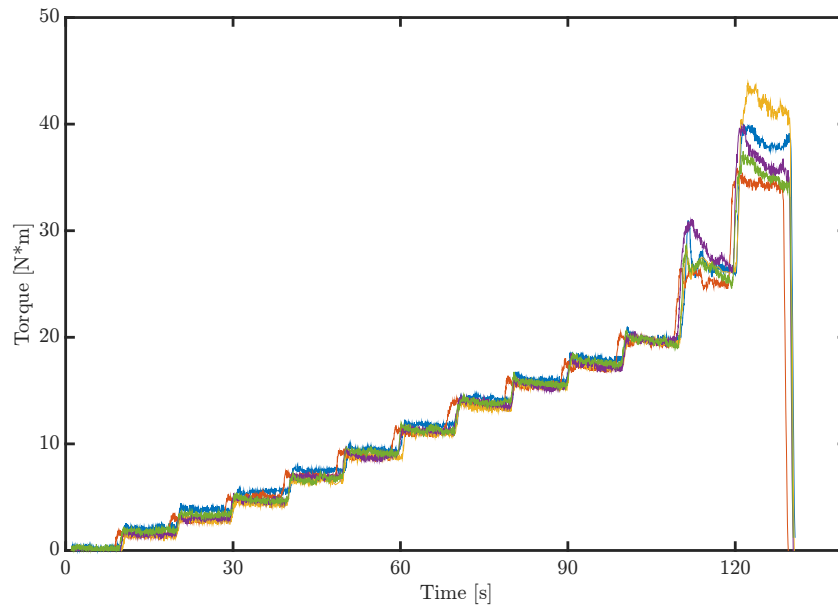
Figure 8-4: Prosthesis ankle torque at various angles (92 degrees at t = 0 s to 80 degrees at t = 120 s) at 11 year old setting. N = 5.
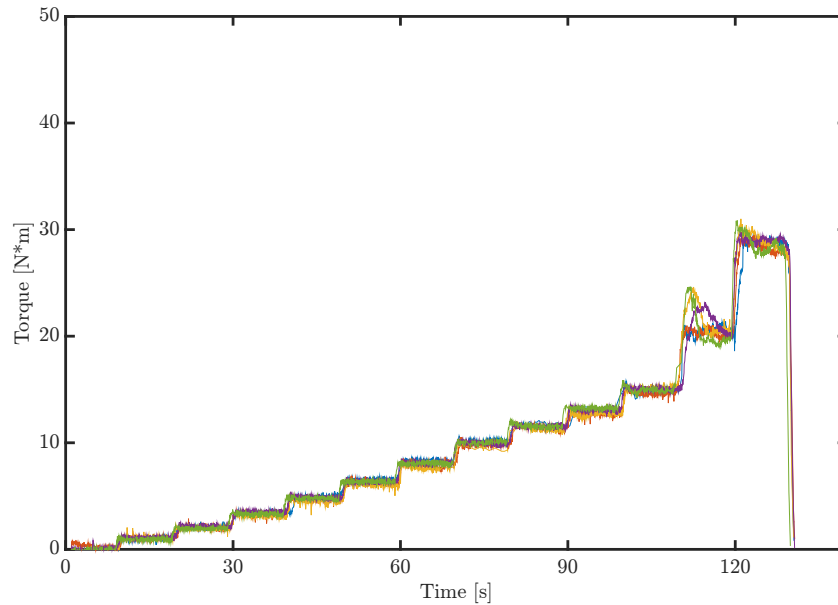
8.2.3 Analysis

First, the raw data was averaged over the five trials to determine the mean torque output at each of the 12 angles (92 to 80 degrees in increments of 1 degree). This data was plotted against the torque vs angle profile predicted by the model as well as the biological torque vs angle profile, as seen in Figure 8-5. Error bars represent the standard deviation of the data. 92 degrees is represented as a 0 degree displacement from resting position, with each decreasing ankle angle as an increasing degree of displacement.
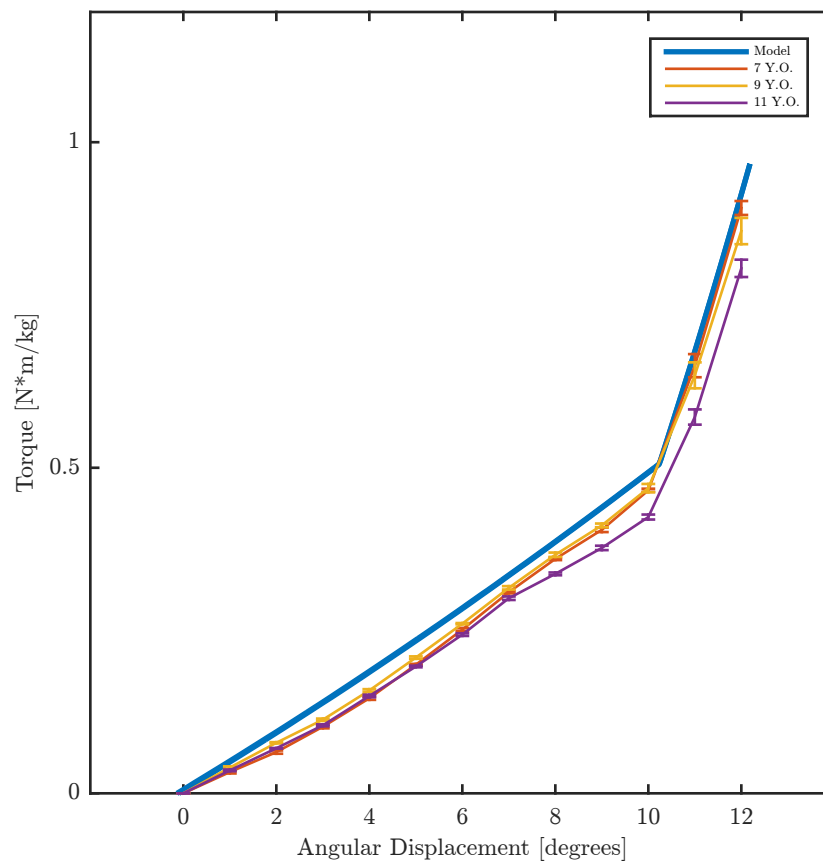
Figure 8-5: Ankle torque generated by prosthesis at range of angles observed during stance phase compared to modeled and biological ankle.

The results show that all three age settings output less torque than the model predicts (less-than-optimal spring constants), though the 7 and 9 year old settings

69

perform better than the 11 year old.

8.3 Dynamic Testing

8.3.1 Protocol

During dynamic testing, the ankle angle was displaced over the same range but at a constant angular velocity. A video recording of the experiment was used to determine the actual angular velocity of the ankle joint. Only the 7 year old case was tested, since the damping coefficient remains constant between the settings.

8.3.2 Data

Figure 8-6 shows the raw data from the iPecs load cell time-synced with the ankle measurement obtained from video analysis in Logger Pro. The data seen is for a 7 year old, over five flexion-extension cycles.
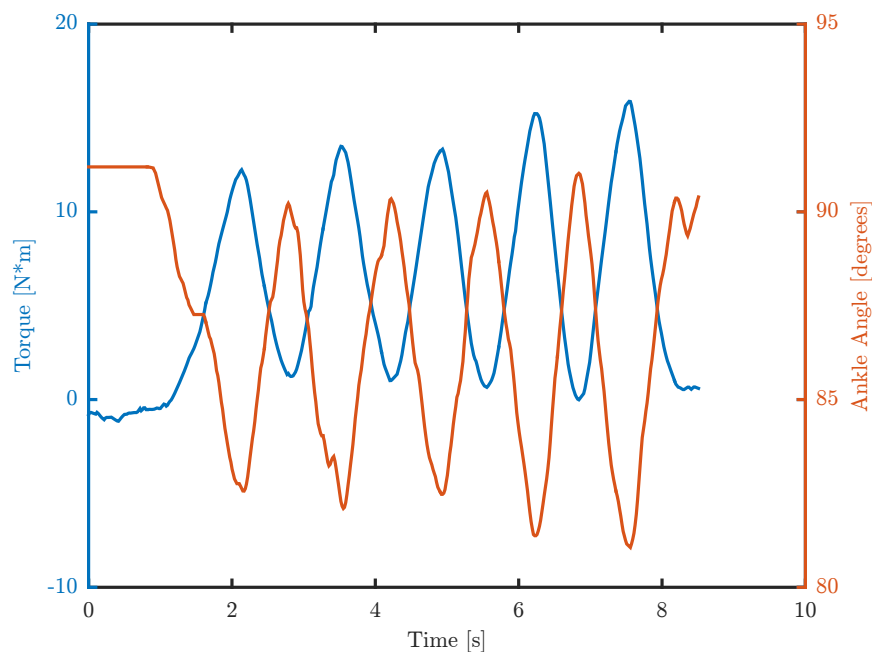
Figure 8-6: Raw torque data from iPecs load cell and angle data from video analysis during dynamic testing of prosthesis (7 year old setting).

8.3.3 Analysis

First, the raw angle data was analyzed to determine the average instantaneous angular velocity across trials at all angles. In order to increase the certainty of the first assumption, only the velocity measurements between 83 and 88 degrees at increments of 1 degree (a portion of the overall ankle angle range) were recorded.

Next, the average of the torques recorded in each of the six angles (between 83 and 88 degrees) was determined. Due to the damping effect, the torques during flexion were different from the those during extension, even in the same angle interval.

Figure 8-7 shows the torque produced at each of the angles between 83 and 88 degrees, compared to what was predicted by the MATLAB model. An ankle angle of 88 degrees is represented by 4 degrees of displacement from resting position, while 83 degrees is represented by 9 degrees of displacement.

Figure 8-7: Modeled and experimentally-determined dynamic torque profile for prosthesis (7 year old setting) during flexion and extension. Arrows show direction of ankle angle change.

The results demonstrated that the damping was not consistent throughout the entire range of motion. Figure 8-8 show the model prediction of how the flexion and

extension torques vary as damping coefficient changes.
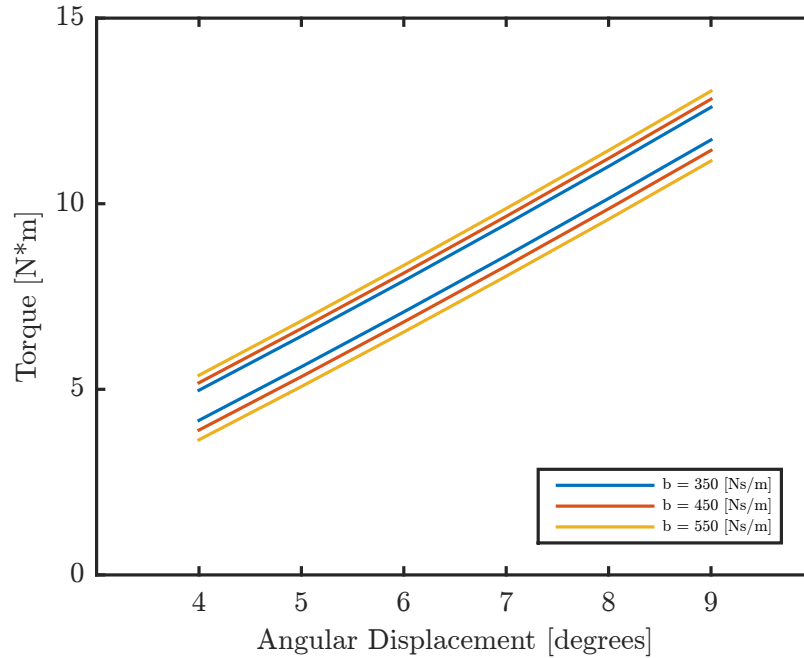
Figure 8-8: Modeled flexion (upper) and extension (lower) torque profiles at various damping coefficients.

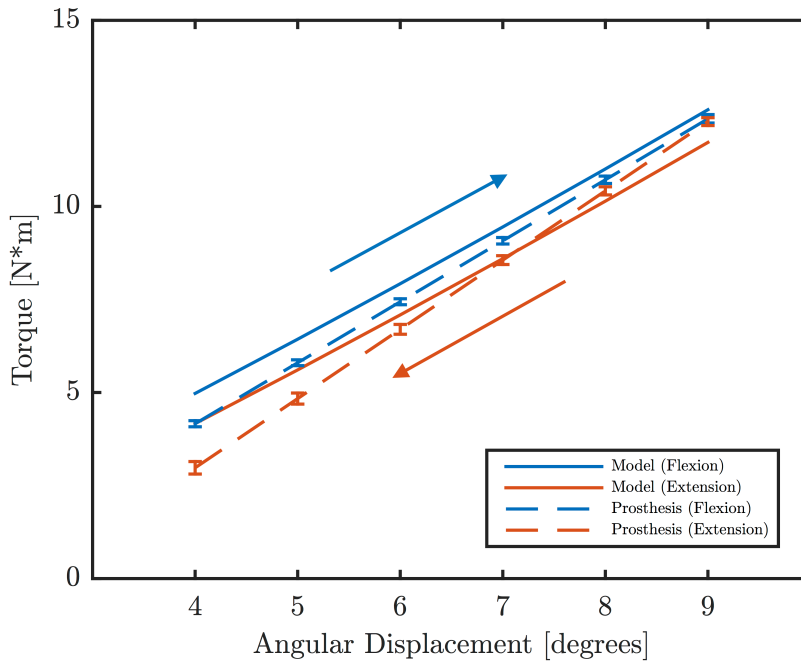As the damping coefficient (b) increases, the difference between the flexion and extension torques increase. The information from Figure 8-8 suggested the damping coefficient decreased as the angular displacement from resting position increased, as seen in Figure 8-7.

The variation in damping seen in Figure 8-7, however, could also be attributed to the fact that the angular velocity, which affects the damping force, was not constant throughout the experiment. To account for this, further calculations were required.

The torque produced by the device at a given ankle angle can be simplified by the following expression: $T(\theta) = k\theta + b(\theta)\dot{\theta}$. Since the spring properties of the device was determined in Section 8.2.3, this information was used, along with the average torque output and instantaneous angular velocity at a given angle, in order to determine the effective damping coefficient (b) at angles between 83 and 88 degrees.

Figure 8-9 shows the calculated damping coefficient at each angle, compared to the constant 350 Ns/m required by the model.
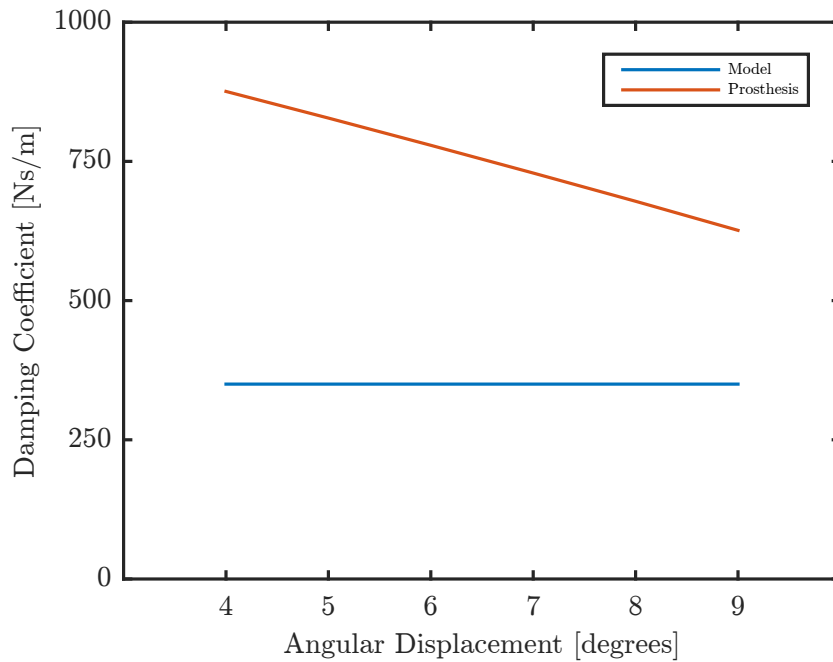
Figure 8-9: Effective damping coefficient of device at various angles compared with model-generated design requirement (350 Ns/m).

In order to predict how the prosthesis would behave on a patient based on the static and dynamic tests, the damping coefficient was selected using a simple average across the 4 to 9 degree angle displacement range (750 Ns/m). Both the estimated damping coefficient, as well as the effective spring constant information determined in Section 8.2.3, were re-integrated into the MATLAB model to generate a predicted dynamic torque profile for each age setting throughout the gait cycle. Figure 8-10 compares the model results to the experimentally determined torque profile.
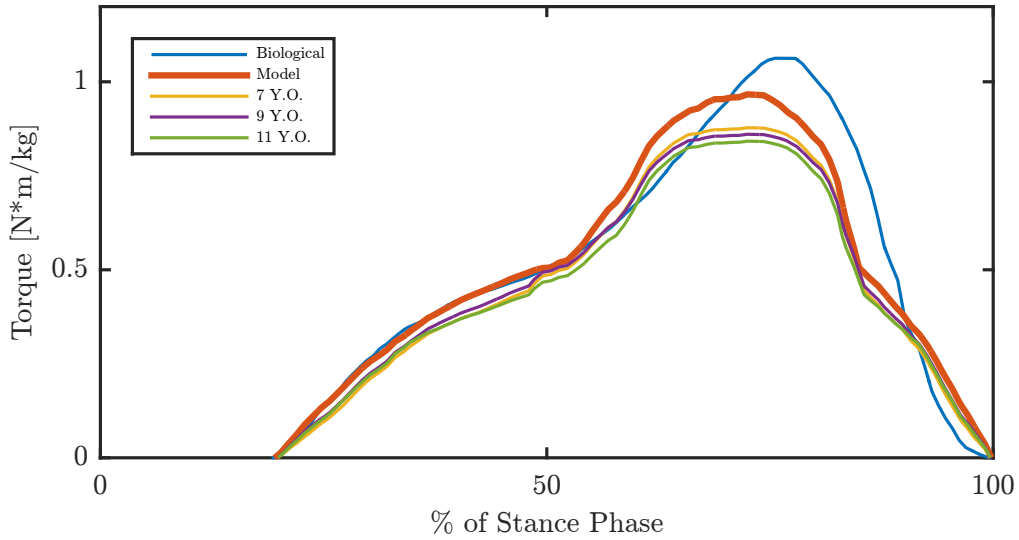
Figure 8-10: Predicted performance of prosthesis compared to modeled and biological ankle.

The results demonstrate that the performance of the device, specifically the torque output, declines as the age setting increases. This decline is minimal during the parts of the stance phase when only the ankle spring is activated, but becomes amplified when the toe spring engages.

Nevertheless, all three age settings were predicted to adequately provide torque during the latter half of the stance phase, when traditional passive devices are unable to deliver sufficient power.

Chapter 9

Conclusion

The purpose for this thesis was to design and construct an affordable prosthesis for pediatric amputees that would not need to be replaced as the patient grew. In addition to being adaptable for children ages 7-11, the constructed prosthesis also promises to drastically improve the resulting gait pattern of patients. By matching the gait profile of a healthy child far better than existing passive devices of similar cost and function, the designed prosthesis will likely reduce co-morbidities, which currently exist in patients using devices that do not provide sufficient power.

Furthermore, the adaptability of this device makes prosthetic solutions significantly more affordable for pediatric patients. While the current cost of the device at scale (n = 500) is \$123, which includes the cost of replacing the ankle springs over the 7-11 age range, potential modifications to the device design and manufacturing techniques promise to further reduce the cost. Exploring ways materials could be sourced through local supply chains, as opposed to manufacturing the devices abroad, could also lead to new materials (alternatives to the carbon fiber spring, for example) and lower cost.

Despite the device's achievements, there is much area of opportunity for improvement. Currently, the torque outputted by the device prototype falls short of what the model predicts the output to be. This shortfall was a result of both insufficient spring stiffness and excessive damping. Both these issues could be resolved in the next iteration of the device's design. The former could be addressed by specifying

new springs, while the latter could be tackled both by adjusting the damping coefficient on the adjustable dashpot as well as incorporating more robust bearings to reduce friction and damping in the device.

Another limitation of this design was the constraints put on the device's age settings. The 7-11 age range was dictated by the anthropometric data available in literature. In order for this device to have a larger impact, its reach should be to a wider range of patients. Collecting more data pertaining to limb specification and gait patterns of younger and older children would help achieve this goal.

In reality, however, even children of the same age may exhibit different segment dimensions and kinetics. These differences could be a result of gender or build. A potential solution to this problem could be to determine the device settings based on weight rather than age. For example, the device could be adjusted every time the child gained 5 kilograms, instead of aging a year. This would ensure that the torque outputs, which in a healthy child typically scale by mass, remain as tailored and accurate as possible.

The most salient component of this project, however, is not the creation of an affordable or even adjustable device. It is the idea that the computer model, which was developed in this project, in tandem with the design of an affordable and adjustable prosthesis, introduces a new paradigm into the field of passive prostheses. Using the model to both understand what healthy gait looks like as well as how a specific prosthesis design affects the resulting gait of users, we can begin to create affordable, accurate, and tailored devices for individuals, who would previously have had to settle with one-size-fits-all passive solutions. This merging of affordability and accuracy promises to substantially increase the access to prostheses for children around the world who most need them.

Chapter 10

Acknowledgements

I would like to thank my mentors, Tyler Clites and Hugh Herr, at the MIT Media Lab for their advice, support, criticism and enthusiasm. They believed in the idea and unrelentingly challeneged me to be a better engineer.

The Harvard SEAS community has been an incredible support system for this project—Maurice Smith, Linsey Moyer, Chris Lombardo, Rob Wood—as well as members of the Teaching Labs—Elaine Kristant, Maddie Hickman, Steve Cortesa.

To all my friends and family who have stood by me every step of the way, both throughout this thesis as well as my Harvard career, much gratitude is owed.

Finally, and most importantly, the inspiration for this project stemmed from my time working at the Cambodia Trust Prosthetic Clinic in Phnom Penh. To the individuals like Carson Harte, Sisary Kheng and Odom Teap, who are pushing to increase the accessibility of prosthetic technology in developing countries, thank you for your perseverance, vision, and kindness.

Appendix A

Bill Of Materials

Part Description	Units	Manufacturer	Part No.	Single Prototype		Bulk (n = 500)	
				Unit Price	Price	Unit Price	Price
Spring	1.000	Lee Spring	LHC 192N 07M	$15.86	$15.86	$2.87	$2.87
Spring	1.000	Lee Spring	LHC 207N 06M	$17.73	$17.73	$3.52	$3.52
Spring	1.000	Lee Spring	LHC 207N 06S	$30.08	$30.08	$8.51	$8.51
Spring Plunger	1.000	McMaster	9657K273	$0.86	$0.86	$0.86	$0.86
Spring Holder Top	1.000	SUNPE	Custom	$80.00	$80.00	$24.20	$24.20
Spring Holder Bottom	1.000	SUNPE	Custom	$52.00	$52.00	$12.50	$12.50
Dashpot	1.000	Airpot	2KS95A2.0NF	$60.00	$60.00	$20.00	$20.00
Foot Pivot Bracket	2.000	McMaster	6498K72	$4.42	$8.84	$4.42	$8.84
Bushing	6.000	McMaster	2706T13	$4.17	$25.02	$0.50	$3.00
Shaft Collar	6.000	McMaster	6432K12	$0.94	$5.64	$0.50	$3.00
Sleeve Bearing	1.000	McMaster	9829K1	$19.66	$19.66	$9.83	$9.83
Stando	1.000	McMaster	91115A516	$2.19	$2.19	$1.86	$1.86
Shank Frame Bracket	4.000	McMaster	1556A65	$1.80	$7.20	$1.34	$5.36
Guide Rail	0.300	McMaster	9829K11	$25.30	$7.59	$8.43	$2.53
U Channel	0.008	McMaster	9001K55	$31.21	$0.24	$31.21	$0.24
Carbon Fiber 48"	0.038	McMaster	2153T25	$28.07	$1.05	$28.07	$1.05
Aluminum 1/4 in 48x48	0.003	McMaster	9037K46	$723.70	$2.08	$723.70	$2.08
Aluminum 1/8 in 48x48	0.022	McMaster	8885K42	$511.11	$11.12	$511.11	$11.12
Aluminum 0.063in	0.007	McMaster	8885K39	$282.40	$2.08	$282.40	$2.08
TOTAL					**$349.24**		**$123.45**

Figure A-1: Bill of materials, single device cost, and bulk cost.
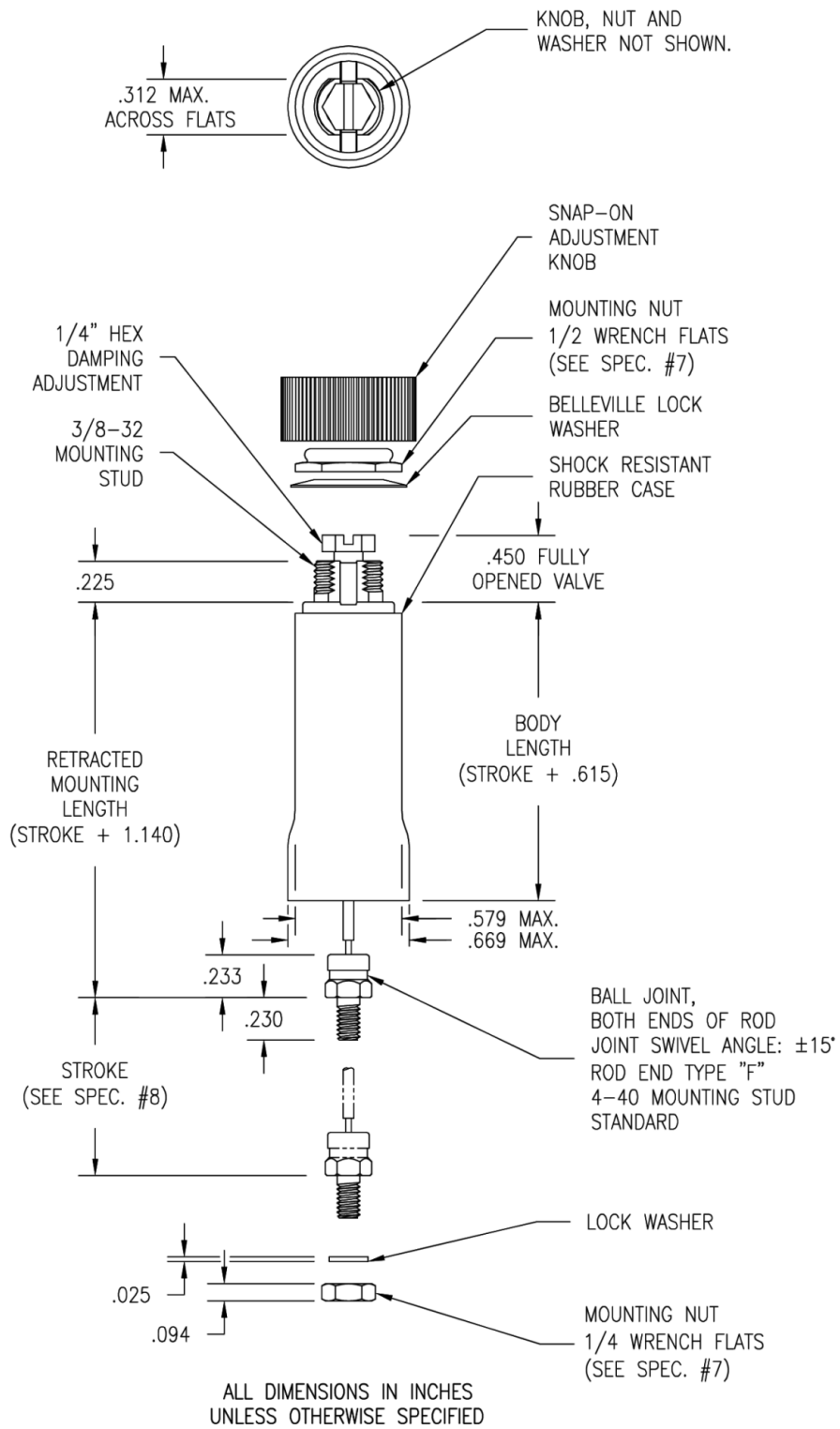
Appendix B

Engineering Drawings
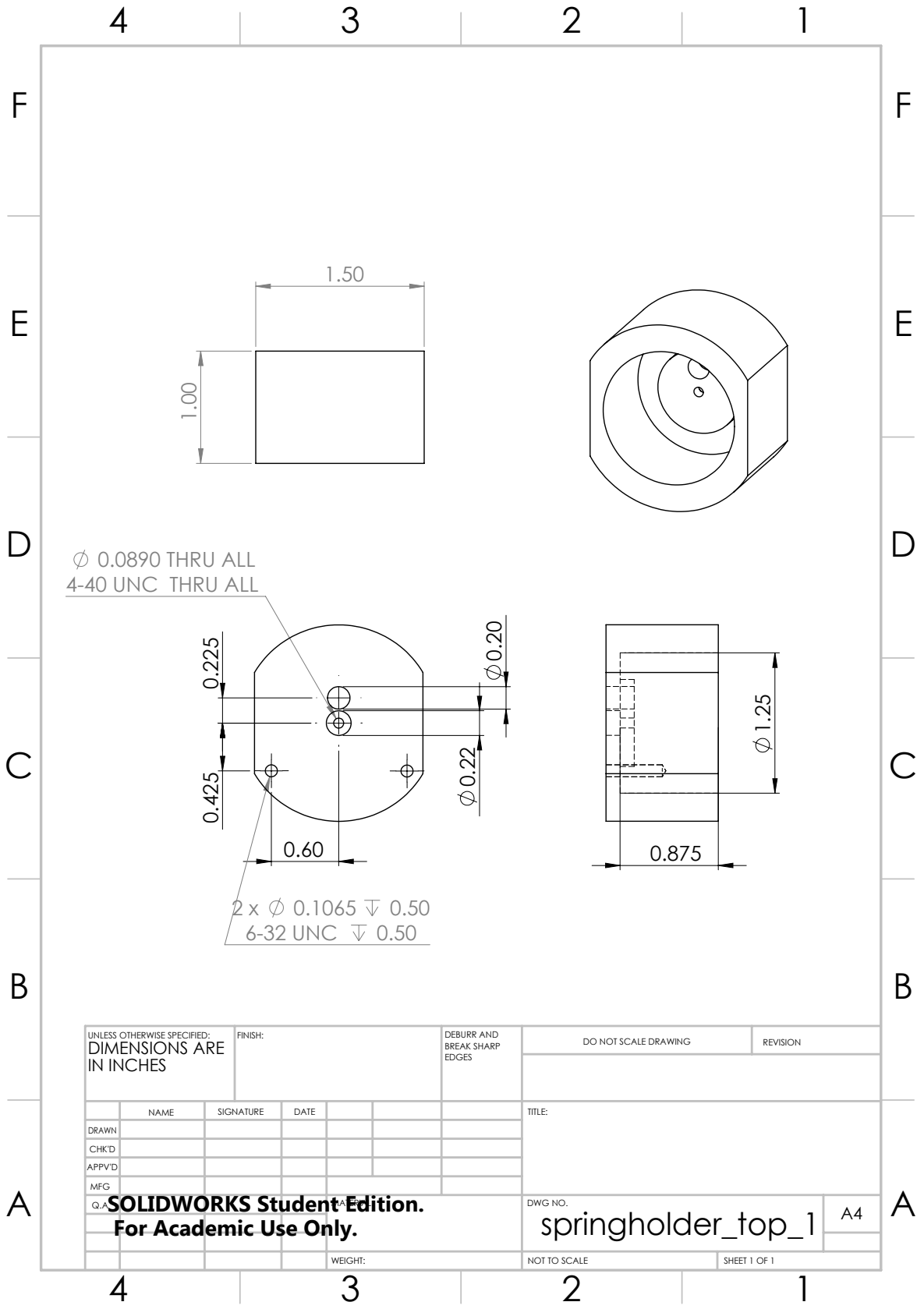
Figure B-1: Airpot 2KS95 dashpot datasheet [25].
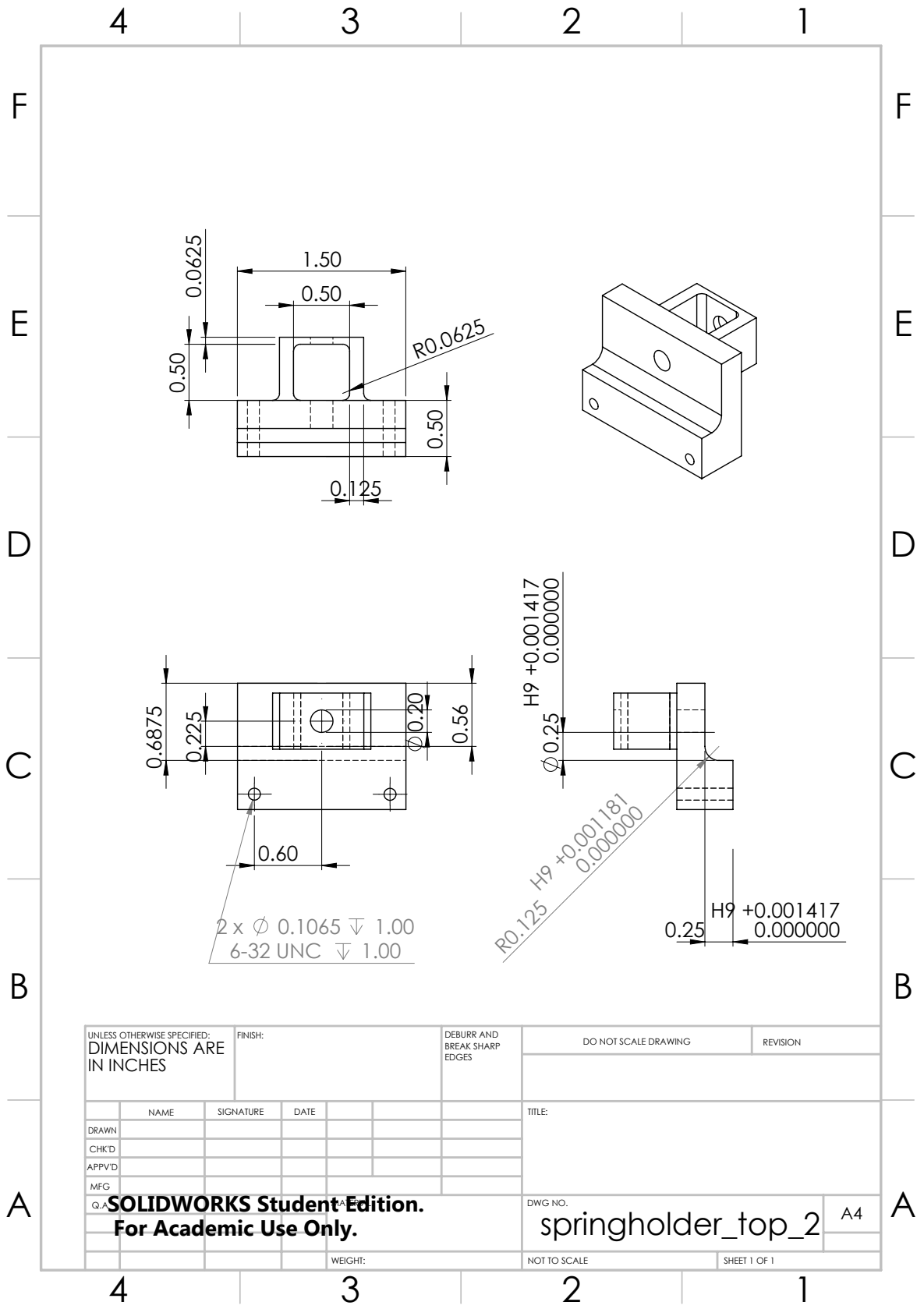
Figure B-2: First component of the upper spring holder.

Figure B-3: Second component of the upper spring holder.

0.50

0.00000
-0.00035
∅0.37500

0.50

0.75

0.375

∅0.775

∅1.25

∅ 0.34 THRU ALL
3/8-24 UNF THRU ALL

∅1.4375

0.125

UNLESS OTHERWISE SPECIFIED: DIMENSIONS ARE IN INCHES	FINISH:			DEBURR AND BREAK SHARP EDGES	DO NOT SCALE DRAWING		REVISION

	NAME	SIGNATURE	DATE			TITLE:		
DRAWN								
CHK'D								
APPV'D								
MFG								
Q.A								

SOLIDWORKS Student Edition.
For Academic Use Only.

DWG NO.
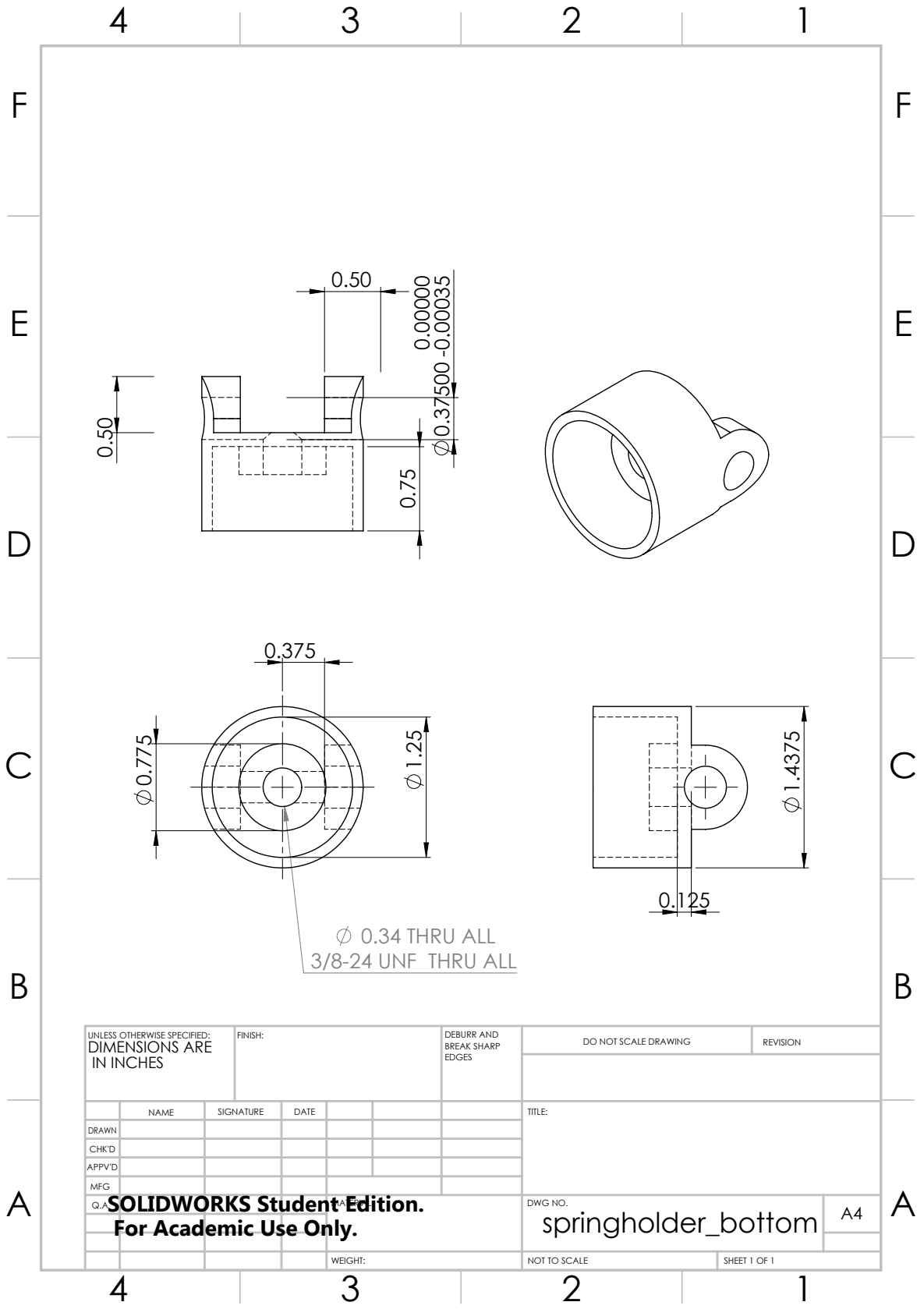springholder_bottom

A4

WEIGHT:

NOT TO SCALE

SHEET 1 OF 1

Figure B-4: Lower spring holder.

Bibliography

[1] W. H. Organization, "Guidelines for training personnel in developing countries for prosthetics and orthotics services," 2005. [Online]. Available: http://apps.who.int/iris/bitstream/10665/43127/1/9241592672.pdf

[2] E. Strait, "Prosthetics in developing countries," *Prosthetic Resident*, pp. 1–40, 2006. [Online]. Available: http://www.doc-developpement-durable.org/file/sante-hygiene-medecine/handicaps/Protheses-Propylene/DevelopingCountries.pdf

[3] "Exceed, Formerly Cambodia Trust, Prosthetics Orthotics, Southeast Asia." [Online]. Available: http://www.exceed-worldwide.org/

[4] S. K. Au and H. M. Herr, "Powered ankle-foot prosthesis," *IEEE Robotics Automation Magazine*, vol. 15, no. 3, pp. 52–59, Sep. 2008.

[5] J. Schwartz, "A Brand-New Kick: The New BiOM Ankle Prosthetic by MIT's Hugh Herr," Dec. 2013. [Online]. Available: http://www.bostonmagazine.com/health/article/2013/11/26/prosthetics-research-boston-biom-ankle-prosthetic/

[6] J. J. Rice, J. M. Schimmels, and S. Huang, "Design and Evaluation of a Passive Ankle Prosthesis With Powered Push-Off," *Journal of Mechanisms and Robotics*, vol. 8, no. 2, pp. 021 012–021 012, Nov. 2015. [Online]. Available: http://dx.doi.org/10.1115/1.4031302

[7] J. M. Schimmels and S. Huang, "Passive ankle prosthesis with energy return simulating that of a natural ankle," USA Patent US 8 721 737 B2, May, 2014. [Online]. Available: https://www.google.com/patents/US8721737

[8] J. Foot, "Stanford-Jaipur Knee," 2016. [Online]. Available: http://jaipurfoot.org/what_we_do/prosthesis/stanford_jaipur_knee.html

[9] D. Grieg, "A \$20 prosthetic knee to bring relief to disadvantaged amputees," Apr. 2009. [Online]. Available: http://newatlas.com/a-20-prosthetic-knee-to-bring-relief-to-disadvantaged-amputees/11514/

[10] C. Staff, "Continental Innovators: Jaipur Foot," Apr. 2015. [Online]. Available: http://blog.continentalcurrency.ca/innovators-jaipur-foot/

[11] "Foot Design." [Online]. Available: https://www.limbsinternational.org/technology-development/13837/Foot-Design

[12] M. Windrich, M. Grimmer, O. Christ, S. Rinderknecht, and P. Beckerle, "Active lower limb prosthetics: a systematic review of design issues and solutions," *BioMedical Engineering OnLine*, vol. 15, no. 3, p. 140, 2016. [Online]. Available: http://dx.doi.org/10.1186/s12938-016-0284-9

[13] Ossur, "Standard Adapters," 2016. [Online]. Available: https://www.ossur.com/prosthetic-solutions/products/all-products/standard-adapters

[14] K. J. Ganley and C. M. Powers, "Anthropometric parameters in children: a comparison of values obtained from dual energy x-ray absorptiometry and cadaver-based estimates," *Gait & Posture*, vol. 19, no. 2, pp. 133–140, Apr. 2004. [Online]. Available: http://www.sciencedirect.com/science/article/pii/S0966636203000389

[15] P. J. McNair and H. Prapavessis, "Normative data of vertical ground reaction forces during landing from a jump," *Journal of Science and*

Medicine in Sport, vol. 2, no. 1, pp. 86–88, Mar. 1999. [Online]. Available: http://www.sciencedirect.com/science/article/pii/S144024409980187X

[16] G. A. Cavagna, P. Franzetti, and T. Fuchimoto, "The mechanics of walking in children." *The Journal of Physiology*, vol. 343, pp. 323–339, Oct. 1983. [Online]. Available: http://www.ncbi.nlm.nih.gov/pmc/articles/PMC1193922/

[17] J. Foot, "Fabrication Processes and Materials," 2016. [Online]. Available: http://jaipurfoot.org/how_we_do/fabrication_processes.html

[18] "Fundamentals of Human Gait," Dec. 2016. [Online]. Available: http://musculoskeletalkey.com/fundamentals-of-human-gait/

[19] S. M. S. Ounpuu, J. R. M. D. Gage, and R. B. Davis, "Three-Dimensional Lower Extremity Joint Kinetics in Normal Pediatric Gait," *Journal of Pediatric Orthopaedics*, vol. 11, no. 3, pp. 341–349, Jun. 1991.

[20] R. Beardmore, "Leaf Springs," 2008. [Online]. Available: http://www.roymech.co.uk/Useful_Tables/Springs/Springs_Leaf.html

[21] "Carbon Fiber Bars." [Online]. Available: https://www.mcmaster.com/

[22] "Spring Polymagnet pair - Long Range Repel." [Online]. Available: http://catalog.polymagnet.com/featured-products/1002290.html

[23] "Belleville Disc Spring Stack Design Calculator," 2009. [Online]. Available: http://www.meadinfo.org/2009/07/belleville-disc-spring-stack-design.html

[24] Spirol, "Spirol Disc Springs." [Online]. Available: https://www.spirol.com/library/main_catalogs/SPIROL-Disc-Springs-us.pdf

[25] "Stock Dashpot Model 95." [Online]. Available: http://airpot.com/product/stock-dashpot-model-95/

[26] "Compression Spring Catalog." [Online]. Available: http://www.leespring.com/browse_catalog.asp?springType=C

[27] "6061 Aluminum Bars." [Online]. Available: https://www.mcmaster.com/